

Improved empirical parametrizations of the $\gamma^*N \rightarrow \Delta(1232)$ and $\gamma^*N \rightarrow N(1520)$ transition amplitudes and the Siegert's theorem

G. Ramalho

*International Institute of Physics, Federal University of Rio Grande do Norte,
Campus Lagoa Nova - Anel Viário da UFRN, Lagoa Nova, Natal-RN, 59070-405, Brazil*
(Dated: June 1, 2016)

In the nucleon electroexcitation reactions, $\gamma^*N \rightarrow R$, where R is a nucleon resonance (N^*), the electric amplitude E , and the longitudinal amplitude $S_{1/2}$, are related by $E \propto \frac{\omega}{|\mathbf{q}|} S_{1/2}$, in the pseudo-threshold limit ($|\mathbf{q}| \rightarrow 0$), where ω and $|\mathbf{q}|$ are respectively the energy and the magnitude of three-momentum of the photon. The previous relation is usually refereed to as the Siegert's theorem. The form of the electric amplitude, defined in terms of the transverse amplitudes $A_{1/2}$ and $A_{3/2}$, and the explicit coefficients of the relation, depend on the angular momentum and parity (J^P) of the resonance R . The Siegert's theorem is the consequence of the structure of the electromagnetic transition current, which induces constraints between the electromagnetic form factors in the pseudo-threshold limit. In the present work, we study the implications of the Siegert's theorem for the $\gamma^*N \rightarrow \Delta(1232)$ and $\gamma^*N \rightarrow N(1520)$ transitions. For the $\gamma^*N \rightarrow N(1520)$ transition, in addition to the relation between electric amplitude and longitudinal amplitude, we also obtain a relation between the two transverse amplitudes: $A_{1/2} = A_{3/2}/\sqrt{3}$, at the pseudo-threshold. The constraints at the pseudo-threshold are tested for the MAID2007 parametrizations of the reactions under discussion. New parametrizations for the amplitudes $A_{1/2}$, $A_{3/2}$ and $S_{1/2}$, for the $\gamma^*N \rightarrow \Delta(1232)$ and $\gamma^*N \rightarrow N(1520)$ transitions, valid for small and large Q^2 , are proposed. The new parametrizations are consistent with both: the pseudo-threshold constraints (Siegert's theorem) and the empirical data.

I. INTRODUCTION

The information relative to the structure of the electromagnetic transition between the nucleon and a nucleon excitation R ($\gamma^*N \rightarrow R$), can be parametrized in terms of helicity amplitudes dependent on the photon polarization states, and the transfer momentum squared q^2 , which is restricted to the region $Q^2 = -q^2 > 0$ [1, 2]. For the transitions $\frac{1}{2}^+ \rightarrow \frac{1}{2}^\pm, \frac{3}{2}^\pm$, where J^P represents the state of angular momentum J , parity $P = \pm$, and $\frac{1}{2}^+$ is the nucleon state, one can define the transverse amplitudes $A_{1/2}$, $A_{3/2}$ and the longitudinal or scalar amplitude $S_{1/2}$ ($A_{3/2}$ can be defined only for $J = \frac{3}{2}$).

Although those amplitudes are in principle independent functions, there are relations between them in the limit where the photon momentum $|\mathbf{q}|$ vanishes. This limit is called the pseudo-threshold limit, corresponding to the case where both the nucleon and the resonance R are at rest. At the pseudo-threshold limit ($|\mathbf{q}| = 0$), one has $Q^2 = -\omega^2$, where $\omega = M_R - M$ is the photon energy, and M_R , M are respectively the resonance and the nucleon masses. Since the pseudo-threshold limit is defined by $Q^2 = Q_{PS}^2 < 0$, with $Q_{PS}^2 = -(M_R - M)^2$, it belongs to the unphysical region, where the helicity amplitudes cannot be measured from the $\gamma^*N \rightarrow R$ transition. The extension of models for the $Q^2 < 0$ region is important, however, for studies of reactions such as the Δ Dalitz decay ($\Delta \rightarrow e^+e^-N$) and Dalitz decays of other resonances [3, 4].

At the pseudo-threshold the matrix element of the elec-

tric multipole E , defined by the spatial current density \mathbf{J} , and the matrix element of the Coulomb multipole $S_{1/2}$, defined by the charge density ρ , can be related by $E \propto \frac{\omega}{|\mathbf{q}|} S_{1/2}$ [5]. This result, obtained in the limit of the long wavelengths ($|\mathbf{q}| \rightarrow 0$), is usually refereed as the Siegert's theorem [5–9]. Although defined below $Q^2 = 0$, the relations between amplitudes can be used to test analytic properties of theoretical models and to test the consistency of phenomenological parametrizations.

The exact proportionality between the electric amplitude E and the scalar amplitude $S_{1/2}$ depends on the angular momentum-parity state (J^P) of the resonance. The constraints for the helicity amplitudes can in general be derived from the analysis of the transition currents, expressed in a covariant form in terms of the properties of the nucleon and the resonance, which define a minimal number of independent structure form factors [10–12].

In Ref. [13], the implications of the pseudo-threshold limit for the $\gamma^*N \rightarrow N(1535)$ transition form factors and helicity amplitudes, and their implications in the parametrizations of the data are discussed in detail. In the present work we discuss the consequences of the pseudo-threshold limit for the $\gamma^*N \rightarrow \Delta(1232)$ and $\gamma^*N \rightarrow N(1520)$ transitions.

For the $\gamma^*N \rightarrow \Delta(1232)$ transition, we will conclude that, in the pseudo-threshold limit, one has $\frac{E}{|\mathbf{q}|} = \sqrt{2}\omega \frac{S_{1/2}}{|\mathbf{q}|^2}$, where $\omega = M_R - M$, and M_R is the Δ mass. Note that the previous relation differs from the usual form $E = \sqrt{2}\omega \frac{S_{1/2}}{|\mathbf{q}|}$ [14, 15], by a factor $1/|\mathbf{q}|$. This dif-

ference has implications in shape of the parametrizations of the data, as we will show. [Along the paper, we will interpret the factors like $S_{1/2}/|\mathbf{q}|$ or $S_{1/2}/|\mathbf{q}|^2$, as functions defined also for $|\mathbf{q}| = 0$, with the result given by the limit $|\mathbf{q}| \rightarrow 0$, when the limit exists.]

As for the $\gamma^*N \rightarrow N(1520)$ transition, the pseudo-threshold limit induces two constraints in the helicity amplitudes. The trivial constraint is expressed as $\frac{1}{2}E = \sqrt{2}\frac{\omega}{|\mathbf{q}|}S_{1/2}$, where ω is now defined in terms of the $N(1520)$ mass (M_R). In addition, one has also the relation $A_{1/2} = A_{3/2}/\sqrt{3}$, at the pseudo-threshold.

The explicit form of the electric and the scalar amplitudes will be defined later for cases $\frac{3}{2}^+$ and $\frac{3}{2}^-$. Defining $\lambda_R = \sqrt{2}(M_R - M)$, we can express the correlation between the electric and scalar amplitudes (Siegert's theorem) as $\frac{E}{|\mathbf{q}|} = \lambda_R \frac{S_{1/2}}{|\mathbf{q}|^2}$ for the $\gamma^*N \rightarrow \Delta(1232)$ transition, and $\frac{1}{2}E = \lambda_R \frac{S_{1/2}}{|\mathbf{q}|}$ for the $\gamma^*N \rightarrow N(1520)$ transition.

In order to take into account the constraints from the pseudo-threshold limit, in this work we present new parametrizations of the $\gamma^*N \rightarrow \Delta(1232)$ and $\gamma^*N \rightarrow N(1520)$ helicity amplitudes. We will conclude at the end, that, an overall description of the data for low Q^2 and large Q^2 , including the pseudo-threshold, is possible using smooth representations of the helicity amplitudes. The presented parametrizations are compared with the MAID2007 parametrizations [14–16]. Parametrizations for very large Q^2 , that simulate the expected falloff from perturbative QCD (pQCD), will be proposed.

This article is organized as follows: In Sec. II, we discuss the formalism associated with the electromagnetic transition current, helicity amplitudes and transition form factors. In Secs. III and IV, we study the $\gamma^*N \rightarrow \Delta(1232)$ and $\gamma^*N \rightarrow N(1520)$ transitions, respectively. Parametrizations of the data appropriate for very large Q^2 are discussed In Sec. V. Finally in Sec. VI, we present our summary and conclusions.

II. GENERALITIES

We introduce now the formalism associated with the $\gamma^*N \rightarrow R$ transition, where N is the nucleon ($J^P = \frac{1}{2}^+$) and R is a $J^P = \frac{3}{2}^\pm$ resonance. The case $J^P = \frac{3}{2}^+$ corresponds to the $\Delta(1232)$ resonance; the case $J^P = \frac{3}{2}^-$ corresponds to the $N(1520)$ resonance. The variable M_R represents the mass of the resonance under discussion [$\Delta(1232)$ or $N(1520)$].

We start with the discussion of the relation between the electromagnetic transition current and the helicity amplitudes. Next, we look for the properties of the amplitude $S_{1/2}$. Before discussing in detail the transitions $\gamma^*N \rightarrow \Delta(1232)$ and $\gamma^*N \rightarrow N(1520)$, we present some useful notation.

A. Electromagnetic current and helicity amplitudes

In general, the $\gamma^*N \rightarrow R$ transitions can be characterized in terms of transition form factors, to be defined later, or by the helicity amplitudes defined at the resonance rest frame. At the R rest frame, the initial (P_-) and final (P_+) momenta can be represented, choosing the photon momentum, $q = P_+ - P_-$, along the z -axis, as

$$\begin{aligned} P_- &= (E_N, 0, 0, -|\mathbf{q}|), & P_+ &= (M_R, 0, 0, 0) \\ q &= (\omega, 0, 0, |\mathbf{q}|). \end{aligned} \quad (2.1)$$

In the previous equations, $|\mathbf{q}|$ is the magnitude of the photon (and nucleon) three-momentum, given by

$$|\mathbf{q}| = \frac{\sqrt{Q_+^2 Q_-^2}}{2M_R}, \quad (2.2)$$

with $Q_\pm^2 = (M_R \pm M)^2 + Q^2$. The nucleon energy $E_N = \sqrt{M^2 + |\mathbf{q}|^2}$ and the photon energy $\omega = M_R - E_N$ can be expressed covariantly as $E_N = \frac{M_R^2 + M^2 + Q^2}{2M_R}$ and $\omega = \frac{M_R^2 - M^2 - Q^2}{2M_R}$ respectively.

The transverse ($A_{1/2}, A_{3/2}$) and the longitudinal ($S_{1/2}$) amplitudes, are defined at the R rest frame [2, 17], as

$$A_{1/2} = \sqrt{\frac{2\pi\alpha}{K}} \left\langle R, S'_z = +\frac{1}{2} \left| \varepsilon_+ \cdot J \right| N, S_z = -\frac{1}{2} \right\rangle, \quad (2.3)$$

$$A_{3/2} = \sqrt{\frac{2\pi\alpha}{K}} \left\langle R, S'_z = +\frac{3}{2} \left| \varepsilon_+ \cdot J \right| N, S_z = +\frac{1}{2} \right\rangle, \quad (2.4)$$

$$S_{1/2} = \sqrt{\frac{2\pi\alpha}{K}} \left\langle R, S'_z = +\frac{1}{2} \left| \varepsilon_0 \cdot J \right| N, S_z = +\frac{1}{2} \right\rangle \frac{|\mathbf{q}|}{Q}, \quad (2.5)$$

where S'_z (S_z) is the final (initial) spin projection, $Q = \sqrt{Q^2}$, ε_λ^μ ($\lambda = 0, \pm 1$) are the photon polarization vectors, and J^μ is the electromagnetic transition current operator in units of the elementary charge e . In addition, $\alpha = \frac{e^2}{4\pi} \simeq 1/137$ is the fine-structure constant and $K = \frac{M_R^2 - M^2}{2M_R}$.

The properties associated with the structure of the resonance R are then encoded in the electromagnetic transition current operator J^μ . In the case of a transition between a spin $\frac{1}{2}$ state (N) and a spin $\frac{3}{2}$ state (R) we can project the current into the asymptotic states using

$$\begin{aligned} J_{NR}^\mu &\equiv \langle R | J^\mu | N \rangle \\ &= \bar{u}_\alpha(P_+) \Gamma^{\alpha\mu}(P, q) u(P_-), \end{aligned} \quad (2.6)$$

where u_α and u are respectively the Rarita-Schwinger and the Dirac spinors, $P = \frac{1}{2}(P_+ + P_-)$, and $\Gamma^{\alpha\mu}$ is an operator dependent of the parity, to be defined in the following sections for the case of the $\Delta(1232)$ (positive parity) and the $N(1520)$ (negative parity).

B. Scalar amplitude

In the case of the current conservation, one can replace $(\varepsilon_0 \cdot J) \frac{|\mathbf{q}|}{Q} \rightarrow J^0$, in the definition of the scalar amplitude (2.5), and write

$$S_{1/2} = \sqrt{\frac{2\pi\alpha}{K}} \langle J^0 \rangle, \quad (2.7)$$

where the brackets represent the projection into the spin states with $S'_z = S_z = +\frac{1}{2}$, defined at the resonance rest frame. If the current is not conserved, or the current operator is truncated, we cannot use Eq. (2.7), as discussed in Refs. [5, 18].

Using Eq. (2.7), we can conclude that the scalar amplitude, near the pseudo-threshold, can be expressed for $J^P = \frac{3}{2}^\pm$ cases, as

$$S_{1/2} \propto G_5^P (\bar{u}_3 \mathbb{1}_P u) |\mathbf{q}|, \quad (2.8)$$

where G_5^\pm is a form factor (dependent on the parity \pm), to be defined later, and $\mathbb{1}_P$ is a parity-dependent operator, given by $\mathbb{1}_+ = \gamma_5$ and $\mathbb{1}_- = \mathbb{1}$.

Using the properties of Dirac and Rarita-Schwinger spinors, we can conclude that $(\bar{u}_3 \gamma_5 u) = \sqrt{\frac{2}{3}} \frac{|\mathbf{q}|}{2M} \propto |\mathbf{q}|$ and $(\bar{u}_3 u) = -\sqrt{\frac{2}{3}} = \mathcal{O}(1)$, near the pseudo-threshold [19, 20]. Applying those results, one obtains $S_{1/2} = \mathcal{O}(|\mathbf{q}|^2)$ for $\Delta(1232)$ resonance and $S_{1/2} = \mathcal{O}(|\mathbf{q}|)$ for $N(1520)$ resonance.

Note that, the result $\langle J^0 \rangle \propto G_5^\pm |\mathbf{q}|^n$, with $n = 2$ for positive parity, and $n = 1$, for negative parity, leads to $\langle J^0 \rangle \rightarrow 0$, in the pseudo-threshold limit, if the form factor G_5^\pm has no singularities in this limit, as expected [11]. The result $\langle J^0 \rangle = 0$ is equivalent to the orthogonality between the nucleon and the resonance states. The same property can be observed in the $\gamma^* N \rightarrow N(1535)$ transition, where $N(1535)$ is a $J^P = \frac{1}{2}^-$ state [13].

It is interesting to note that, the dependence of a function $F(Q^2)$, near the pseudo-threshold, can be inferred directly from the graph of the function in terms of Q^2 . Since the derivative in Q^2 , can be determined by the derivative in $|\mathbf{q}|$, given by

$$\frac{dF}{dQ^2} = \frac{M_R^2 + M^2 + Q^2}{4M_R^2 |\mathbf{q}|} \frac{dF}{d|\mathbf{q}|}, \quad (2.9)$$

we conclude that, at the pseudo-threshold (limit $|\mathbf{q}| \rightarrow 0$), the derivative $\frac{dF}{dQ^2}$ will be infinite (vertical line), when $F = \mathcal{O}(|\mathbf{q}|)$, and finite, only when $F = \mathcal{O}(|\mathbf{q}|^n)$ with $n \geq 2$ (we are interested only in the natural powers n). To summarize: the graphs with an infinite derivative at the pseudo-threshold are the representation of functions $\mathcal{O}(|\mathbf{q}|)$; the graphs with finite derivative at the pseudo-threshold represent functions $\mathcal{O}(|\mathbf{q}|^n)$ with $n \geq 2$.

C. Notation

In the following sections, we will study separately the resonances $\Delta(1232)$ and $N(1520)$. To convert helicity amplitudes into form factors, we use the factor [2, 17, 21]

$$F_\pm = \frac{1}{e} \frac{2M}{M_R \pm M} \sqrt{\frac{MM_R K}{Q_\mp^2}}. \quad (2.10)$$

The factor F_+ will be used for the case $\frac{3}{2}^+$, and the factor F_- will be used for the case $\frac{3}{2}^-$. For convenience we also define $\tau = \frac{Q^2}{(M_R + M)^2}$.

In the next two sections, we will also define the magnetic, electric and scalar amplitudes: $M_{l\pm}$, $E_{l\pm}$ and $S_{l\pm}$, where $l = J \mp 1/2$ is an integer and $P = \pm$ is the parity, for the case $J = 3/2$. For a more detailed discussion about the multipole amplitude notation see Refs. [11, 15].

III. $\gamma^* N \rightarrow \Delta(1232)$ TRANSITION

The $\gamma^* N \rightarrow \Delta(1232)$ transition current can be determined using Eq. (2.6), with the operator [2, 11, 12, 19]

$$\begin{aligned} \Gamma^{\alpha\mu}(P, q) = & \\ G_1 q^\alpha \gamma^\mu \gamma_5 + G_2 q^\alpha P^\mu \gamma_5 + G_3 q^\alpha q^\mu \gamma_5 - G_4 g^{\alpha\mu} \gamma_5, & \end{aligned} \quad (3.1)$$

where G_i ($i = 1, \dots, 4$) are structure form factors dependent on Q^2 . The four form factors are not all independent, only three of them are independent. Using the current conservation condition, $q \cdot J = 0$, we can conclude that [19, 20]

$$G_4 = (M_R + M)G_1 + \frac{1}{2}(M_R^2 - M^2)G_2 - Q^2 G_3. \quad (3.2)$$

Instead of the *elementary* form factors G_i , alternatively we can use the multipole form factors: magnetic dipole (G_M), electric quadrupole (G_E) and Coulomb quadrupole (G_C), defined as [12, 19, 20]

$$\begin{aligned} G_M = & Z_R \left[(M_R - M)G_5 + 4MG_1 \right. \\ & \left. + \frac{4M_R^2 |\mathbf{q}|^2}{Q_+^2} \left(\frac{G_1}{2M_R} - G_3 \right) \right], \end{aligned} \quad (3.3)$$

$$\begin{aligned} G_E = & Z_R \left[(M_R - M)G_5 \right. \\ & \left. - \frac{4M_R^2 |\mathbf{q}|^2}{Q_+^2} \left(\frac{G_1}{2M_R} + G_3 \right) \right], \end{aligned} \quad (3.4)$$

$$\begin{aligned} G_C = & Z_R \left[2M_R G_5 \right. \\ & \left. + \frac{4M_R^2 |\mathbf{q}|^2}{Q_+^2} \left(\frac{1}{2} G_2 - G_3 \right) \right], \end{aligned} \quad (3.5)$$

where $Z_R = \frac{2M}{3(M_R + M)}$ and

$$G_5 = G_1 + \frac{1}{2}(M_R + M)G_2 + (M_R - M)G_3, \quad (3.6)$$

is a new auxiliary form factor.

For convenience Eqs. (3.3)-(3.5) are expanded in powers of $|\mathbf{q}|$. For the sake of the discussion, we consider G_1, G_2 and G_3 , as our base for the form factors, following Jones and Scadron [12], but we use also G_4 and G_5 , when necessary. For the multipole form factors we choose the Jones and Scadron representation. To convert to the alternative Ash representation, the functions G_M, G_E and G_C should be divided by the factor $\sqrt{1+\tau}$ [15].

The helicity amplitudes (2.3)-(2.5) can be obtained from the form factors [2, 15], using

$$A_{1/2} = \frac{1}{4F_+}(G_M - 3G_E), \quad (3.7)$$

$$A_{3/2} = -\frac{\sqrt{3}}{4F_+}(G_M + G_E), \quad (3.8)$$

$$S_{1/2} = \frac{1}{\sqrt{2}F_+} \frac{|\mathbf{q}|}{2M_R} G_C, \quad (3.9)$$

where F_+ is defined by Eq. (2.10).

The multipole amplitudes M_{1+}, E_{1+}, S_{1+} , can be defined directly in terms of the multipole form factors, or as a combination of the amplitudes [11, 15],

$$\begin{aligned} G_M &= F_+ M_{1+} \\ &\equiv -F_+(A_{1/2} + \sqrt{3}A_{3/2}), \end{aligned} \quad (3.10)$$

$$\begin{aligned} G_E &= F_+ E_{1+} \\ &\equiv -F_+(\frac{1}{\sqrt{3}}A_{3/2} - A_{1/2}), \end{aligned} \quad (3.11)$$

$$\frac{|\mathbf{q}|}{2M_R} G_C = F_+ S_{1+} \equiv \sqrt{2}F_+ S_{1/2}. \quad (3.12)$$

The multipole amplitudes have the same dimensions as the helicity amplitudes. In this work we define the multipole amplitudes with the sign of the form factors. Other authors use different conventions of sign for the multipole amplitudes [11, 15].

A. Pseudo-threshold limit

Now we consider the pseudo-threshold limit. Since the form factors G_i ($i = 1, 2, 3$), are defined with no kinematic singularity, we can conclude from Eqs. (3.4)-(3.5) that [12]

$$G_E = (M_R - M)Z_R G_5, \quad G_C = 2M_R Z_R G_5, \quad (3.13)$$

when $|\mathbf{q}| \rightarrow 0$. A simple consequence of this result [12], is

$$G_E = \frac{M_R - M}{2M_R} G_C. \quad (3.14)$$

To express the relation (3.14) in terms of helicity amplitudes, we use the relations (3.11)-(3.12) and $F_+ = \frac{1}{e} \frac{M}{M_R + M} \sqrt{\frac{MKQ_+^2}{M_R}} \frac{1}{|\mathbf{q}|}$, and obtain

$$\frac{E_{1+}}{|\mathbf{q}|} = \lambda_R \frac{S_{1/2}}{|\mathbf{q}|^2}. \quad (3.15)$$

In the previous relation we recall that $\lambda_R = \sqrt{2}(M_R - M)$ and $E_{1+} = A_{1/2} - \frac{1}{\sqrt{3}}A_{3/2}$. Note in Eq. (3.15), that the common factor, $1/|\mathbf{q}|$, cannot be eliminated, unless we can prove that $E_{1+} \propto |\mathbf{q}|^n$ and $S_{1/2} \propto |\mathbf{q}|^{(n+1)}$, with $n \geq 2$, near the pseudo-threshold.

The relation (3.15) is consistent with

$$E_{1+} = \mathcal{O}(|\mathbf{q}|), \quad S_{1/2} = \mathcal{O}(|\mathbf{q}|^2), \quad (3.16)$$

near the pseudo-threshold. The previous forms were adopted by the MAID2007 parametrization [16]. As for the amplitude M_{1+} , the MAID2007 parametrization gives $M_{1+} = \mathcal{O}(|\mathbf{q}|)$, near the pseudo-threshold [which is equivalent to $G_M = \mathcal{O}(1)$]. The behavior of the multipole amplitudes near the pseudo-threshold is consistent with the results expected when the form factors G_i are free of kinematic singularities at the pseudo-threshold [10, 11].

To satisfy the condition (3.15), it is necessary that both sides of the equation give the same numerical value. It is at that point that the MAID2007 parametrization fails, as we will show next.

To summarize: we conclude that the correlation between the form factors at the pseudo-threshold given by Eq. (3.14), usually refereed as the Siegert's theorem, is not equivalent to the condition $E_{1+} = \lambda_R \frac{S_{1/2}}{|\mathbf{q}|}$. The equivalent condition is the one expressed by Eq. (3.15).

The results of the MAID2007 parametrization for the form factors G_E and κG_C , where $\kappa = \frac{M_R - M}{2M_R}$, are presented in the top panel of Fig. 1, in comparison with the data from Ref. [22]. The database from Ref. [22] includes data for finite Q^2 from Refs. [23–25], and the world data average of G_E at $Q^2 = 0$, extracted from the particle data group (PDG) result for G_E/G_M at $Q^2 = 0$ [26].

From the top panel of Fig. 1, we can conclude, that, although the MAID2007 describes well the data for G_E and G_C , it fails to describe the relation (3.14). In the graph it is clear that $\kappa G_C(Q_{PS}^2) > G_E(Q_{PS}^2)$. We discuss now alternative parametrizations of the form factors G_E and G_C , that are consistent with the Siegert's theorem expressed in the form (3.14).

B. Improved parametrizations of G_E and G_C

A parametrization consistent with Eq. (3.14), inspired in the MAID2007 form is

$$G_E = \frac{C_0}{K} b_0 (1 + b_1 Q^2 + b_2 Q^4 + b_3 Q^6) e^{-b_4 Q^2} G_D \quad (3.17)$$

$$G_C = \frac{C_0}{K} \frac{2M_R}{K} c_0 (1 + c_1 Q^2 + c_2 Q^4 + c_3 Q^6) e^{-c_4 Q^2} G_D, \quad (3.18)$$

where $G_D = (1 + Q^2/0.71)^{-2}$ is a dipole form factor, and $C_0 = \frac{1}{e} \left(\frac{M^3 K}{M_R} \right)^{1/2}$. The parameters $(b_0, b_1, b_2, b_3, b_4)$ and (c_1, c_3, c_3, c_4) are adjustable. There are two main differences between the MAID2007 expressions and our expressions, apart from the constraint at pseudo-threshold

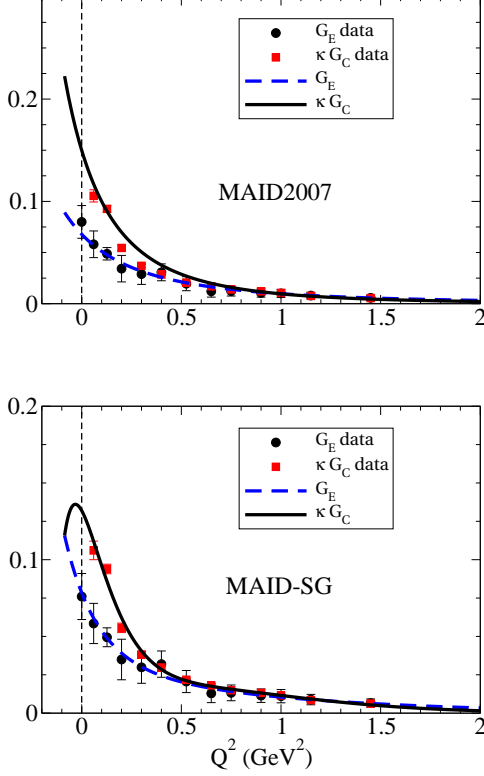


FIG. 1: Electric and Coulomb quadrupole form factors for the $\gamma^*N \rightarrow \Delta(1232)$ transition. G_C is multiplied by $\kappa = \frac{M_R - M}{2M_R}$. At the top: MAID2007 parametrization. At the bottom: improved parametrization MAID-SG, consistent with the Siegert's theorem. Data from Ref. [22] (see description in the text).

discussed previously. The first difference is that we omitted the factor $\sqrt{1 + \tau}$, in Eqs. (3.17)-(3.18). This factor appears in the MAID2007 parametrization because the form factors were defined originally in the Ash representation, and not in the Jones and Scadron representation (conversion factor) [12]. The second difference is the suppression of a factor $1/(1 + dQ^2/(4M^2))$, where d is a new parameter, used in the MAID2007 parametrization of the function G_C . This factor was added to the MAID2007 parametrization in an attempt to improve the quality of the fit near $Q^2 = 0$ [9, 15]. We choose not to include that factor to avoid possible singularities in the timelike region, and also because the inclusion of higher powers in Q^2 , as the terms associated with the coefficients c_2 and c_3 , may be sufficient to simulate the effect of an extra monopole factor in Q^2 (in MAID2007: $c_2 = c_3 = 0$).

Apart from the two differences discussed above, the relevant difference between the present forms and the MAID2007 parametrization is that the coefficient c_0 is fixed by Eq. (3.14), once defined the remaining coefficients. We label the improved parametrization given by Eqs. (3.17)-(3.18), as the MAID-SG parametrization, since the new parametrization is consistent with the Siegert's theorem (SG holds for Siegert).

MAID-SG	r_0	r_1	r_2	r_3	r_4
G_E	14.72	-0.0566	1.91	0.0164	1.31
G_C	21.82	4.38	-13.54	22.54	3.33
MAID2007	r_0	r_1	r_2	r_3	r_4
G_E	12.74 Z_1	-0.021	-	-	0.16
G_C	24.80 Z_2	0.12	-	-	0.23

TABLE I: $\gamma^*N \rightarrow \Delta(1232)$ transition. At the top: parameters used in the calculation of the form factors in the MAID-SG parametrization. At the bottom: parameters used in the MAID2007 parametrization. The labels r_l ($l = 0, 1, 2, 3, 4$) hold for $r_l = b_l, c_l$. r_0 is in units $10^{-3} \text{ GeV}^{-1/2}$ ($C_0/K = 5.32 \text{ GeV}^{1/2}$). r_1 and r_4 are in units GeV^{-2} , r_2 is in units GeV^{-4} and r_3 is in units GeV^{-6} . In the MAID-SG parametrization the value of c_0 (at bold) is determined by Eq. (3.14). In the MAID2007 parametrization, the coefficients r_0 are corrected by the functions $Z_1 = \sqrt{1 + \tau}$ and $Z_2 = 1/(1 + 4.9Q^2/(4M^2))Z_1$.

The coefficients defined by the best fit of the functions (3.17)-(3.18) to the $Q^2 \leq 2 \text{ GeV}^2$ data, are presented in the Table I. The coefficients associated with the MAID2007 parametrization are also included in the table. Note, however, that only the coefficients r_0 can be directly compared, since different combinations of polynomials and exponentials may lead to similar functions.

The results for the MAID-SG parametrization for the form factors G_E and G_C are presented in the lower panel of Fig. 1. At this point we restrict the calculations to the region $Q^2 \leq 2 \text{ GeV}^2$, since the main goal at the moment is the study of parametrizations consistent with the Siegert's theorem, near $Q^2 = Q_{PS}^2 \simeq -0.09 \text{ GeV}^2$. For larger Q^2 there are discrepancies between the data from different groups [20, 25], which are not relevant for the discussion near the pseudo-threshold. In Fig. 1, one can see that the MAID-SG parametrization is consistent with the data from Ref. [22] and with the Siegert's theorem. Note that, compared to the MAID2007 parametrization, the MAID-SG parametrization, gives smaller values for G_C near the pseudo-threshold.

In order to check in more detail the implications of Eq. (3.14), instead of looking for the form factors, we compare the MAID-SG parametrization with the data for $R_{EM} = -\frac{G_E}{G_M}$ and $R_{SM} = -\frac{|\mathbf{q}|}{2M_R} \frac{G_C}{G_M}$. To calculate G_M we use the MAID2007 parametrization, since it gives a very good description of the data and it is unconstrained at the pseudo-threshold. The results for the ratios R_{EM} and R_{SM} are presented in Fig. 2. In addition to the previous data, we present also the MAID data [15]. In the figure, one note the different behavior between the MAID2007 parametrization and the MAID-SG parametrization. Part of this difference is a consequence of the discrepancy between the MAID data and the data used in our fit [22]. We note, however, that, even the MAID2007 parametrization has problems in describing the MAID data for R_{SM} below 1 GeV^2 .

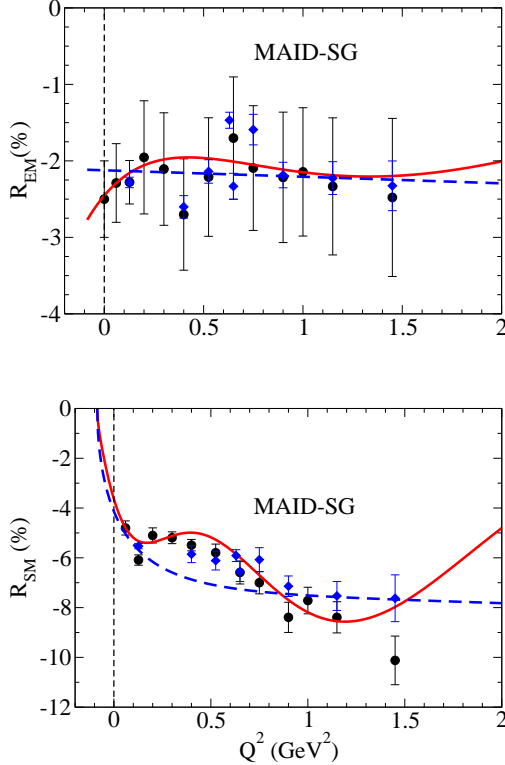


FIG. 2: $\gamma^*N \rightarrow \Delta(1232)$ transition. Ratios R_{EM} and R_{SM} compared with the MAID-SG (solid line) and MAID2007 (dashed line) parametrizations. The data is from the MAID analysis (diamonds) [15] and from the Ref. [22] (circles).

From Figs. 1 and 2, we can conclude, that, the MAID-SG parametrization gives a very good description of the low Q^2 data ($Q^2 < 1 \text{ GeV}^2$) for G_E and G_C . Both functions are smooth near the pseudo-threshold. Looking in more detail in Fig. 2, we see that the MAID-SG parametrization starts to fail when $Q^2 > 1 \text{ GeV}^2$ for R_{SM} . As for R_{EM} , one can see that the function starts to decrease in magnitude for $Q^2 > 2 \text{ GeV}^2$. One can also note, that the data for R_{EM} is well approximated by a constant (similar to MAID2007). The failure of the parametrization for larger values of Q^2 , is in part a consequence of the inclusion of exponential functions in the parametrization of the form factors.

The disadvantage of the use of parametrizations based on exponential factors is that those parametrizations are not valid, in general, for large interval in Q^2 , or fail when Q^2 increases. Latter on, in Sec. V, we discuss the possibility of extending the parametrization of the data for large Q^2 .

We checked, however, if we can improve the description of the large Q^2 region ($Q^2 > 2 \text{ GeV}^2$), by enlarging the range of the data used in the fit to $Q^2 = 3 \text{ GeV}^2$, or $Q^2 = 4.1 \text{ GeV}^2$. Overall, we can improve the description of the data for $Q^2 > 1 \text{ GeV}^2$, but the description for the low Q^2 region losses quality. In particular the result for $G_E(0)$

is overestimated (R_{EM} is underestimated), compared to the PDG result [$G_E(0) = 0.076 \pm 0.015$ and $R_{EM}(0) = -(2.5 \pm 0.5)\%$] [26]. Note that, when we extend the range of the fit for larger values of Q^2 , up to 3 GeV^2 or 4.1 GeV^2 , we reduce the impact of the low Q^2 region in our fit, which leads to a poor estimate of the form factors near the pseudo-threshold. We may then conclude, that, with the parametrizations (3.17)-(3.18), we can not describe well the low and the large Q^2 regions simultaneously. For this reason we restrict, for now, our analysis to the low Q^2 region.

It is worth to mention, that, the fit based on Eqs. (3.17)-(3.18), is very sensitive to the low Q^2 data, in particular to the result at the photon point from PDG [26]. If the datapoint from PDG is replaced by another datapoint, or the errorbar is reduced in the fit, the results for the form factors may change significantly. We note in particular that, in some experiments like in Ref. [27], the value of R_{EM} is larger in absolute value, $R_{EM}(0) = -(3.07 \pm 0.36)\%$.

The Siegert's theorem was already investigated in the context of the $\gamma^*N \rightarrow \Delta(1232)$ transition, within the quark model framework [5, 18, 28–30]. It was found that the Siegert's theorem can be violated when the operators associated with the current density or the charge density are truncated, or expanded in different orders, inducing a violation of the current conservation condition [5, 18, 28]. From those studies, one can conclude that a consistent calculation, where the current is conserved, requires the inclusion of processes beyond the impulse approximation at the quark level (one-body currents), and that, the inclusion of higher order processes involving two-body currents, such as processes with quark-antiquark states and/or meson cloud contributions, is necessary to ensure the conservation of the transition current and the Siegert's theorem [5]. Since the Siegert's theorem is defined at the pseudo-threshold, when $Q^2 \simeq -0.09 \text{ GeV}^2$, one may then conclude, that, processes beyond the impulse approximation are fundamental to describe the helicity amplitudes and the transition form factors at low Q^2 .

The last conclusion is particularly important for the $\gamma^*N \rightarrow \Delta(1232)$ transition, since there are strong evidences of importance of the meson cloud effects for all form factors at small Q^2 [1, 2, 19–21, 31]. For the magnetic dipole form factor, G_M , it is known that the meson cloud effects are small for $Q^2 > 2 \text{ GeV}^2$ [1, 2, 19, 20]. As for the quadrupole form factors G_E and G_C , there are indications that the meson cloud contributions may be important up to 4 GeV^2 [20, 32]. The meson cloud contributions for the quadrupole form factors will be discussed in detail in Sec. V C.

It is important to mention that, the distinction between the valence quark degrees of freedom and the non-valence quark degrees of freedom is only well defined in a given framework. Therefore, valence quark contributions in a given model may appear as non-valence quark contributions in another model. One can nevertheless conclude

that, independent of the model, the meson cloud contributions help in general to approach the estimates from quark models to the experimental data.

IV. $\gamma^* N \rightarrow N(1520)$ TRANSITION

The current associated with the $\gamma^* N \rightarrow N(1520)$ transition is determined using Eq. (2.6), with the operator [2, 11, 17]

$$\Gamma^{\alpha\mu}(P, q) = G_1 q^\alpha \gamma^\mu + G_2 q^\alpha P^\mu + G_3 q^\alpha q^\mu - G_4 g^{\alpha\mu}, \quad (4.1)$$

where G_i ($i = 1, \dots, 4$) are structure form factors dependent on Q^2 . As in the case of the $\gamma^* N \rightarrow \Delta(1232)$, the four form factors are not all independent. In this case the current conservation implies that [17]

$$G_4 = (M_R - M)G_1 + \frac{1}{2}(M_R^2 - M^2)G_2 - Q^2 G_3. \quad (4.2)$$

The multipole form factors can be represented [2, 17], as

$$G_M = -Z_R \frac{4M_R |\mathbf{q}|^2}{Q_+^2} G_1, \quad (4.3)$$

$$G_E = -Z_R \left[4(M_R - M)G_5 - \frac{4M_R^2 |\mathbf{q}|^2}{Q_+^2} \left(\frac{G_1}{M_R} + 4G_3 \right) \right], \quad (4.4)$$

$$G_C = -Z_R \left[4M_R G_5 + \frac{4M_R^2 |\mathbf{q}|^2}{Q_+^2} (G_2 - 2G_3) \right], \quad (4.5)$$

where $Z_R = \frac{1}{\sqrt{6}} \frac{M}{M_R - M}$ and

$$G_5 = G_1 + \frac{1}{2}(M_R - M)G_2 + (M_R + M)G_3. \quad (4.6)$$

Once again, the form factors are decomposed in powers of $|\mathbf{q}|$.

The helicity amplitudes can be determined [2, 17] by

$$A_{1/2} = \frac{1}{4F_-} (3G_M - G_E), \quad (4.7)$$

$$A_{3/2} = -\frac{\sqrt{3}}{4F_-} (G_M + G_E), \quad (4.8)$$

$$S_{1/2} = \frac{1}{\sqrt{2}F_-} \frac{|\mathbf{q}|}{2M_R} G_C. \quad (4.9)$$

Similar to the $\Delta(1232)$ case we also can define the am-

plitudes M_{2-}, E_{2-}, S_{2-} [11]

$$G_M = F_- M_{2-} \equiv -F_- \left(\frac{1}{\sqrt{3}} A_{3/2} - A_{1/2} \right), \quad (4.10)$$

$$G_E = F_- E_{2-} \equiv -F_- (A_{1/2} + \sqrt{3} A_{3/2}), \quad (4.11)$$

$$\frac{|\mathbf{q}|}{2M_R} G_C = F_- S_{2-} \equiv \sqrt{2} F_- S_{1/2}. \quad (4.12)$$

A. Pseudo-threshold limit

From Eqs. (4.3)-(4.5), we can conclude that, at the pseudo-threshold [11, 33]

$$G_M = 0, \quad (4.13)$$

$$G_E = \frac{M_R - M}{M_R} G_C. \quad (4.14)$$

In particular, Eq. (4.14) is a consequence of the result

$$G_E = -4(M_R - M)Z_R G_5, \quad G_C = -4M_R Z_R G_5, \quad (4.15)$$

when $|\mathbf{q}| \rightarrow 0$, since the form factors G_i ($i = 1, 2, 3$) have no kinematic singularities at the pseudo-threshold [11].

A consequence of Eq. (4.14) is, that, at the pseudo-threshold

$$\frac{1}{2} E_{2-} = \lambda_R \frac{S_{1/2}}{|\mathbf{q}|}, \quad (4.16)$$

where, as before $\lambda_R = \sqrt{2}(M_R - M)$. As for the result from Eq. (4.13), it implies that

$$A_{1/2} = \frac{1}{\sqrt{3}} A_{3/2}, \quad (4.17)$$

at the pseudo-threshold [see Eq (4.10)].

The relations (4.16) and (4.17) are consistent with the following behavior of the functions near the pseudo-threshold [11]

$$M_{2-} = \mathcal{O}(|\mathbf{q}|^2), \quad E_{2-} = \mathcal{O}(1), \quad S_{1/2} = \mathcal{O}(|\mathbf{q}|). \quad (4.18)$$

The relation for M_{2-} can be derived directly from Eq. (4.3) when $G_1 = \mathcal{O}(1)$. The dependences of M_{2-} and E_{2-} are consistent with the expected result for the transverse amplitudes $A_{1/2}, A_{3/2} = \mathcal{O}(1)$ [10].

Since the available data for the $\gamma^* N \rightarrow N(1520)$ transition at finite Q^2 is restricted to the reactions with proton target we will restrict our analysis to that case.

The results of the MAID2007 parametrization for the amplitudes $A_{1/2}, A_{3/2}$ and $S_{1/2}$ are presented in Fig. 3. At the top, we test the relation (4.16), multiplied by the factor $|\mathbf{q}|$. If the relation is satisfied, the solid line

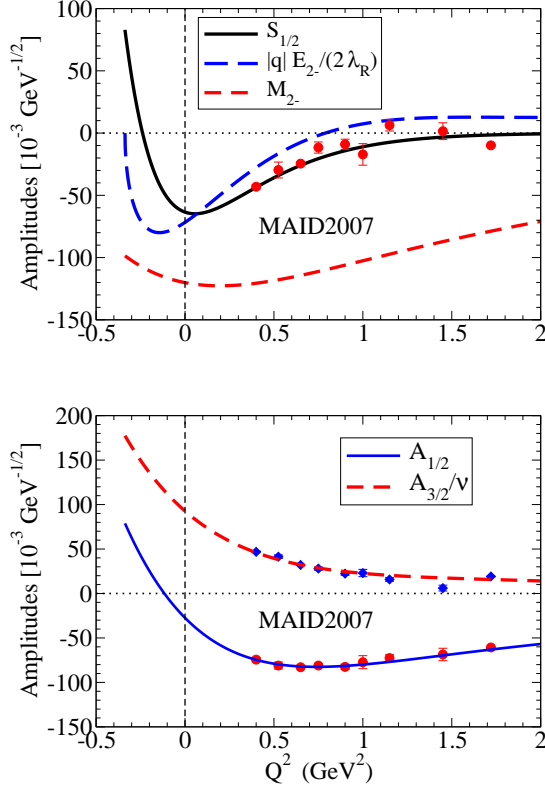


FIG. 3: $\gamma^*N \rightarrow N(1520)$ transition. Results of the MAID2007 parametrization for the amplitudes $A_{1/2}$, $A_{3/2}$ and $S_{1/2}$ (the data represented is for $S_{1/2}$). At the top: $S_{1/2}$ is compared with $|q|E_{2-}/(2\lambda_R)$ and M_{2-} . At the bottom: comparison between $A_{1/2}$ (circles) and $A_{3/2}/\nu$ (diamonds), where $\nu = \sqrt{3}$. Data from the MAID analysis [15, 16].

($S_{1/2}$) and the long-dashed line ($|q|E_{2-}/(2\lambda_R)$) should converge to zero, both, at the pseudo-threshold, when $Q^2 \simeq -0.34 \text{ GeV}^2$. In the same graph we also represent M_{2-} , that should also vanish at the pseudo-threshold, according to Eq. (4.13). At the bottom, we compare $A_{1/2}$ with $A_{3/2}/\sqrt{3}$, in order to test how broken is the relation (4.17), as a consequence of the violation of the condition $M_{2-} = 0$, at the pseudo-threshold.

The results from Fig. 3 show that the relations (4.16) and (4.17), which are consequence of the pseudo-threshold limit (Siegert's theorem), are broken by the MAID2007 parametrization. The failure of the MAID2007 parametrization is then the consequence of the dependences of M_{2-} , E_{2-} , $S_{1/2} = \mathcal{O}(1)$, near the pseudo-threshold. Those dependences are in conflict with the expected dependence of the multipole amplitudes, expressed in Eqs. (4.18). Now we consider alternative parametrizations that are consistent with Eqs. (4.13) and (4.14) [or alternatively by Eqs. (4.16) and (4.17)].

Jlab-SG	r_0	r_1	r_2	r_3	r_4
$A_{1/2}$	-97.40	14.62	-9.49	4.40	1.22
$A_{3/2}$	731.50	0.346	0.0399	1.62	2.32
$S_{1/2}$	-65.17	-0.148	1.01	-	2.46
MAID-SG	r_0	r_1	r_2	r_3	r_4
$A_{1/2}$	-90.43	18.16	-8.61	3.51	1.07
$A_{3/2}$	740.15	-0.443	0.677	-	1.29
$S_{1/2}$	-73.82	-1.26	0.839	-0.185	1.41
MAID2007	r_0	r_1	r_2	r_3	r_4
$A_{1/2}$	-143.37 Z	8.580	-0.252	0.357	1.20
$A_{3/2}$	840.31 Z	-0.820	0.541	-0.016	1.06
$S_{1/2}$	-63.5 X	4.19	-	-	3.40

TABLE II: $\gamma^*N \rightarrow N(1520)$ transition. Parameters used in the calculation of the amplitudes $A_{1/2}$, $A_{3/2}$ and $S_{1/2}$, for the Jlab-SG, MAID-SG and MAID2007 parametrizations. The labels r_l ($l = 0, 1, 2, 3, 4$) hold for $r_l = a_l, b_l, c_l$. r_0 is in units $10^{-3} \text{ GeV}^{-1/2}$, r_1, r_4 are in units GeV^{-2} , r_2 is in units GeV^{-4} and r_3 is in units GeV^{-6} . The values in bold are determined by Eqs. (4.16) and (4.17). In the MAID2007 parametrization, a_0, b_0 are corrected by the function $Z = \sqrt{1 + \tau}$, and c_0 by the function $X = K/|q|$.

B. Improved parametrizations of G_M, G_E and G_C

To obtain parametrizations of the G_M, G_E and G_C data, that include the constraints at the pseudo-threshold, we consider the following representations of the helicity amplitudes

$$A_{1/2} = D a_0 (1 + a_1 Q^2 + a_2 Q^4 + a_3 Q^6) e^{-a_4 Q^2}, \quad (4.19)$$

$$A_{3/2} = D b_0 (1 + b_1 Q^2 + b_2 Q^4 + b_3 Q^6) e^{-b_4 Q^2}, \quad (4.20)$$

$$S_{1/2} = \frac{|q|}{K} c_0 (1 + c_1 Q^2 + c_2 Q^4 + c_3 Q^6) e^{-c_4 Q^2}, \quad (4.21)$$

where $D = K/\sqrt{Q_+^2}$, which can also be written in the form $(M_R + M)D = K/\sqrt{1 + \tau}$. In the expressions (4.19)-(4.21), the coefficients (a_0, a_1, a_2, a_3, a_4), (b_1, b_2, b_3, b_4) and (c_1, c_2, c_3, c_4) are adjustable parameters and b_0, c_0 are determined from the constraints at the pseudo-threshold, once the values of the remaining coefficients are fixed. Since, at the pseudo-threshold, we can write $E_{2-} = -4A_{1/2}$, using Eq. (4.17), we can conclude, that both b_0 and c_0 can be expressed in terms of a_0 [because $A_{3/2} \propto A_{1/2}$ and $S_{1/2}/|q| \propto E_{2-} \propto A_{1/2}$].

In Eqs. (4.19)-(4.20), the factor $1/\sqrt{Q_+^2}$, is included in D for convenience, in order to generate simpler analytic expressions for the form factors G_M, G_E and G_C , after the multiplication by the factor F_- , defined by Eq. (2.10). The conversion into the form factors can be done using Eqs. (4.10)-(4.12). Alternatively we can use parametrizations for the form factors. However, in the present case, the inclusion of the constraints at the pseudo-threshold

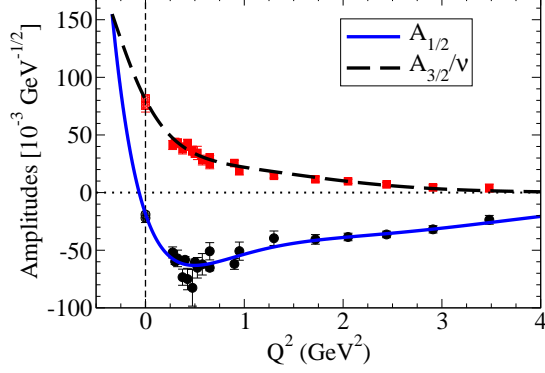


FIG. 4: $\gamma^* N \rightarrow N(1520)$ transition. Results of the Jlab-SG parametrization for the amplitudes $A_{1/2}$ (circles) and $A_{3/2}/\nu$ (squares), where $\nu = \sqrt{3}$. Data from Jlab [25, 35, 36] and Refs. [37, 38] ($Q^2 = 0$).

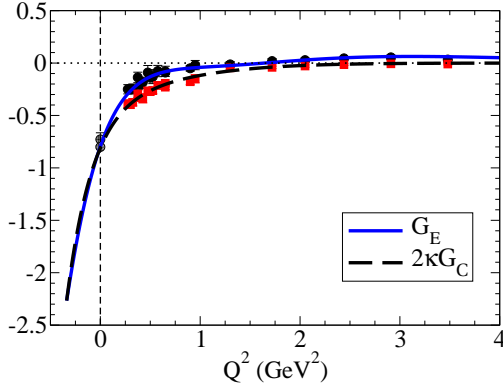


FIG. 5: $\gamma^* N \rightarrow N(1520)$ transition. Results of the Jlab-SG parametrization for the form factors G_E (circles) and G_C (squares) [multiplied by $2\kappa = (M_R - M)/M_R$]. Data from Jlab [25, 35, 36] and Refs. [37, 38] ($Q^2 = 0$).

is simplified when we use the helicity amplitude representation, combined with Eqs. (4.16) and (4.17).

The parametrization (4.19)-(4.21), where $A_{1/2}, A_{3/2} = \mathcal{O}(1)$ and $S_{1/2} = \mathcal{O}(|\mathbf{q}|)$, is compatible with the pseudo-threshold limit, when we impose (4.17), leading to $M_{2-} = \mathcal{O}(|\mathbf{q}|^2)$ [34]. As for the electric amplitude E_{2-} , the result $E_{2-} = \mathcal{O}(1)$, is the direct consequence of the results of the amplitudes $A_{1/2}$ and $A_{3/2}$.

In order to test if the parametrizations (4.19)-(4.21) are compatible with the data, we fitted the coefficients from the expressions (4.19)-(4.21) to the available data.

Apart from the data for $Q^2 = 0$, there are two main datasets available: the data measured at CLAS/Jlab [25, 35, 36], and the data from the MAID analysis [15, 16]. Since there are discrepancies between the results from Jlab and MAID [16, 17], we study the two datasets separately.

There are no data for the region $Q^2 < 0.28 \text{ GeV}^2$, ex-

cept for the measurements at the photon point ($Q^2 = 0$). As a consequence, the fits to the data, and the extrapolation to the pseudo-threshold depend crucially of the data used at $Q^2 = 0$.

Since the average presented by the PDG is affected by a large errorbar, which will leave the region near $Q^2 = 0$ weakly constrained, we take into account only the most recent measurements selected by PDG, presented in Refs. [37, 38].

In the following, we look for possible parametrizations of the data from Jlab and MAID. We analyze first the data from Jlab, defining the Jlab-SG parametrization. Next, we consider the MAID data, deriving the MAID-SG parametrization. At the end we compare the results from the two parametrizations near the pseudo-threshold.

1. Jlab data

We started the fitting process using the Jlab data, combined with the $Q^2 = 0$ data from Refs. [37, 38], as discussed above. The parameters associated with the Eqs. (4.19)-(4.21) are presented in the Table II, under the label Jlab-SG. In the table, r_l ($l = 0, 1, 2, 3, 4$) holds for a_l, b_l and c_l . The values in bold are not the result of the fit. As mentioned, those values are determined by Eqs. (4.16) and (4.17). The coefficients of the MAID2007 parametrization are also presented for comparison. Some Q^2 dependent factors used in MAID2007 are included in the caption.

The results for the Jlab-SG parametrization are presented in Figs. 4, 5, 6 and 7. In Fig. 4, we compare the amplitudes $A_{1/2}$ and $A_{3/2}$. In the figure one can see that $A_{1/2}$ and $A_{3/2}/\sqrt{3}$ have the same value at the pseudo-threshold, as expected from Eq. (4.17). In Fig. 5, we compare the results for G_E and G_C [corrected by the factor $2\kappa = (M_R - M)/M_R$]. It is clear from the figure, that, those form factors have a strong variation near $Q^2 = 0$ (see inflection at low Q^2), and that $G_E = 2\kappa G_C$, at the pseudo-threshold, consistent with the relation (4.14).

In Figs. 4 and 5, we tested directly the constraints of our fit. We can now observe the consequences of the constraints for the remaining functions. In Fig. 6, we show the result of the parametrization for the magnetic form factor G_M . In the graph we can confirm that $G_M = 0$, at the pseudo-threshold, which is the consequence of the relation Eq. (4.17), tested in Fig. 4.

Finally, in Fig. 7, we show the results for the amplitude $S_{1/2}$. Although the information included in $S_{1/2}$ is almost the same as the one included in the form factor G_C , since $G_C \propto (F_-/|\mathbf{q}|)S_{1/2}$, it is interesting to see the behavior near $Q^2 = 0$, and the convergence to zero at the pseudo-threshold.

Overall, the Jlab-SG parametrization gives a very good description of the Jlab data, both at low and large Q^2 . In addition, the Jlab-SG parametrization also provides

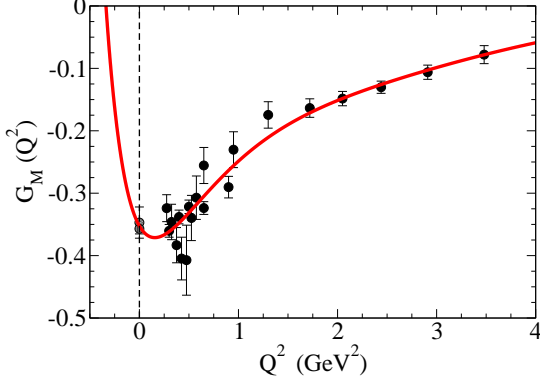


FIG. 6: $\gamma^*N \rightarrow N(1520)$ transition. Results of the Jlab-SG parametrization for the form factor G_M . Data from Jlab [25, 35, 36] and Refs. [37, 38] ($Q^2 = 0$).

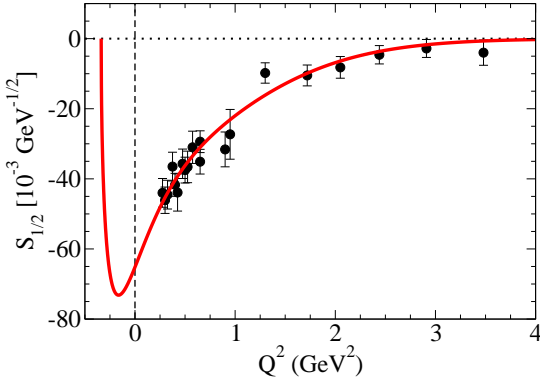


FIG. 7: $\gamma^*N \rightarrow N(1520)$ transition. Results of the parametrization Jlab-SG for the amplitude $S_{1/2}$. Data from Jlab [25, 35, 36].

regular extensions for the region $Q^2 < 0$, including the pseudo-threshold limit.

2. MAID data

We now look for the results from the MAID analysis [15, 16]. We checked if the data can be described by Eqs. (4.19)-(4.21). The results obtained for the coefficients of the fit are presented in the Table II, under the label MAID-SG. Since we concluded already that the relations (4.19)-(4.21) are compatible with the Siegert's theorem, there is no need to test those relations for the new parametrization.

The results of the MAID-SG parametrization for the helicity amplitudes are presented in Fig. 8 and the corresponding results for the form factors are presented in Fig. 9.

Contrary to the case of the Jlab data, it is not possible in this case to obtain a high quality fit, based on the form (4.19)-(4.21). There are two main reasons for

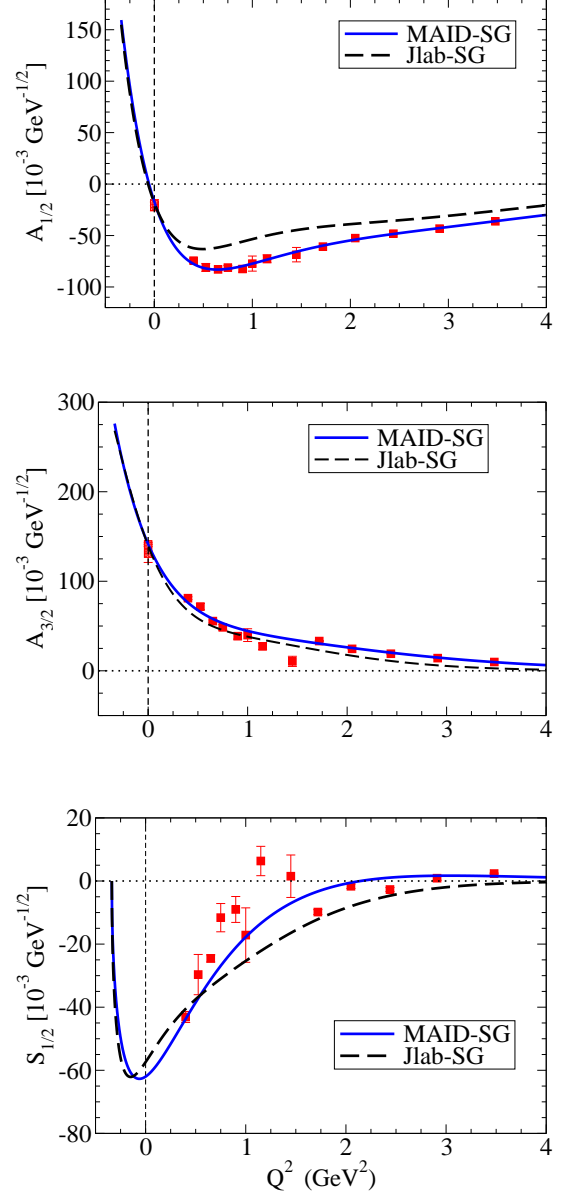


FIG. 8: $\gamma^*N \rightarrow N(1520)$ transition. Results for the MAID-SG amplitudes compared with the MAID data [15, 16]. The Jlab-SG parametrization is also presented.

that. One of the reasons is that the data in the interval $Q^2 = 1.4\text{--}1.8 \text{ GeV}^2$, in the transition between the two MAID datasets [15, 16], shows fluctuations that are not compatible with the simple third order polynomial form, assumed in the present parametrization. The second reason is that the MAID data for $Q^2 > 1.5 \text{ GeV}^2$ [16], have very small errorbars, which impose a strong constrain in the large Q^2 region (dominance of the large Q^2 data in the fit).

We conclude however, that, a high quality fit can be obtained in the region $Q^2 < 1.5 \text{ GeV}^2$ [15]. In this case, the extrapolation for higher Q^2 generates very large con-

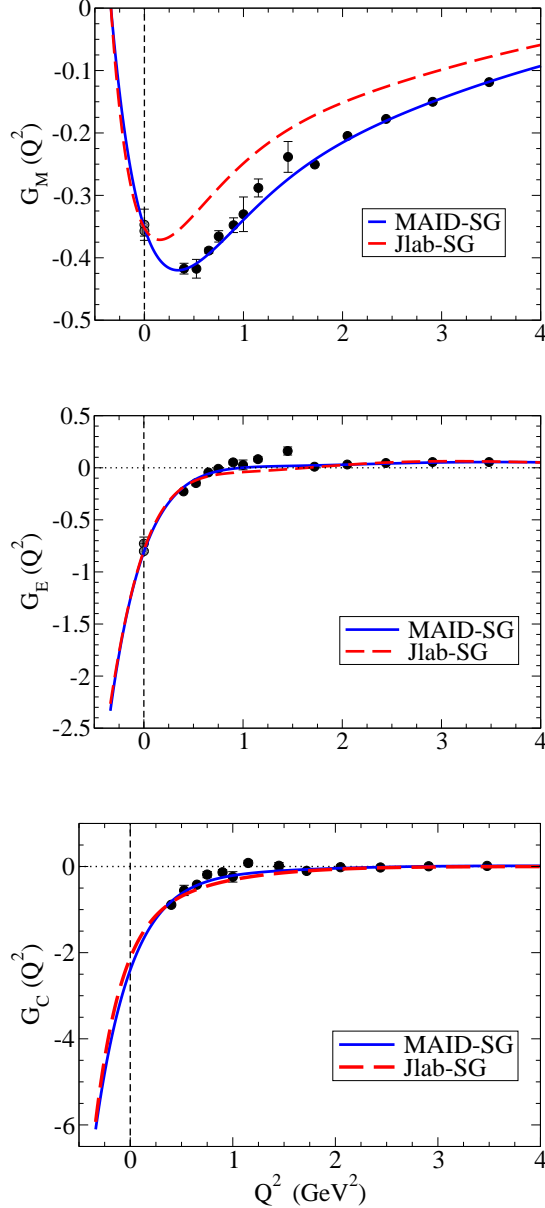


FIG. 9: $\gamma^*N \rightarrow N(1520)$ transition. Results for the MAID-SG form factors compared with the MAID data [15, 16]. The Jlab-SG parametrization is also presented.

tributions for the form factors, that are also incompatible with the MAID data for the region $Q^2 > 1.5 \text{ GeV}^2$ [16]. As in the case of $\gamma^*N \rightarrow \Delta$ quadrupole form factors, it is not possible to derive a parametrization appropriated simultaneously for small and large Q^2 , based on functions with exponential factors. Alternative parametrizations will be discussed in Sec. V.

In Figs. 8 and 9, we can observe that the MAID-SG parametrization describes very well the $A_{1/2}$ and the G_M data. As for the amplitudes $A_{3/2}$ and $S_{1/2}$, one can observe some fluctuations of the data in the region $Q^2 = 1.4\text{--}1.8 \text{ GeV}^2$. As already discussed, those fluctu-

ations are the reason why it is not possible to obtain a very accurate description of the MAID data. The result obtained for the amplitude $S_{1/2}$ differs significantly from the MAID2007 parametrization. The poor description of the MAID data given by the MAID-SG parametrization is a consequence of trying to describe the data and be consistent with the Siegert's theorem, at the same time. The fluctuations of the data in region $Q^2 = 1.4\text{--}1.8 \text{ GeV}^2$, and the deviation from the fit can also be seen in the graphs for the form factors G_E and G_C . In any case, if we look for the helicity amplitudes, or for the form factors, the MAID-SG parametrization describes well the large Q^2 region.

In the Figs. 8 and 9, we also include the results of the parametrization Jlab-SG. We avoid to include the Jlab data for a question of legibility, but, we recall that the Jlab-SG parametrization follows closely the Jlab data. From the comparison between the MAID-SG and Jlab-SG parametrizations, we can conclude, that, the two parametrizations, although very different for $Q^2 > 1 \text{ GeV}^2$, have a very similar behavior near the pseudo-threshold.

3. Discussion

From the analysis of the Jlab and MAID data, we already noticed, that both parametrizations lead to very similar extensions for the $Q^2 < 0$ region. We may be tempted to conclude, that, the closeness between the two parametrizations for small Q^2 is essentially the consequence of the data considered at the photon point. This conclusion is however incorrect. The inclusion of the more recent CLAS data, with three datapoints in the region $Q^2 = 0.65\text{--}1.30 \text{ GeV}^2$ [36], has a significant impact in the Jlab-SG fit. When we include the corresponding data in the fit, the values of the amplitudes $A_{1/2}$ and $A_{3/2}$ increase by 15%, at the pseudo-threshold, and the amplitude $S_{1/2}$ decreases at $Q^2 = 0$ by 13%. In both cases, the amplitudes are modified below the region $Q^2 < 0.3 \text{ GeV}^2$ (the threshold of the data for finite Q^2).

We then conclude that, the behavior near the pseudo-threshold, is not only the consequence of the low Q^2 data, but that the fit is also constrained by data up to 1 GeV^2 . For this reason, it is remarkable that the Jlab-SG and the MAID-SG parametrizations are so close near the pseudo-threshold.

As discussed in Sec. II B, some of the properties near the pseudo-threshold of the amplitudes and form factors can be observed directly in the graphs. In Fig. 8, one can see in the graph for the amplitude $S_{1/2}$, the convergence at the pseudo-threshold, $S_{1/2} \rightarrow 0$, with an infinite derivative (consequence of $S_{1/2} \propto |\mathbf{q}|$). Also in Fig. 9, we can note, in the graph for G_M , that, the derivative of G_M near the pseudo-threshold is finite, as we could anticipate from $G_M = \mathcal{O}(|\mathbf{q}|^2)$.

To finalize the discussion of the $\gamma^*N \rightarrow N(1520)$ transition, it is interesting to discuss the results for the ampli-

tude $A_{3/2}$ in the context of a quark model framework. In Fig. 8, one can see that the amplitude $A_{3/2}$ is very large near $Q^2 = 0$, compared to the amplitude $A_{1/2}$. It is however known that estimates of the meson cloud effects predict in general large contributions for the amplitude $A_{3/2}$ near $Q^2 = 0$, and that the valence quark contributions are only about 1/3 of the total [17, 39–43]. Since $A_{3/2}(0)$ and the extrapolation of the function $A_{3/2}$ for the pseudo-threshold limit, differs significantly, we may conclude that, as for the case of the $\gamma^*N \rightarrow \Delta(1232)$ transition, discussed in Sec. IIIB, the amplitude $A_{3/2}$ is also dominated by processes beyond the impulse approximation. The stronger candidate for those contributions are the meson cloud contributions, as discussed in Ref. [17].

In contrast with the previous discussion are results of the constituent quark model with two-body exchange currents from Ref. [44]. In this model the valence quark contribution is dominant near $Q^2 = 0$ and the non valence quark degrees of freedom contribute to less than 20%.

V. EXTENSION OF THE MAID-TYPE PARAMETRIZATIONS FOR LARGE Q^2

We now discuss alternative parametrizations to the usual MAID parametrizations, which are based on the combination of polynomial and exponential functions of Q^2 (MAID-type parametrizations).

As already discussed, an important disadvantage of the parametrizations based on exponential factors, $e^{-\beta Q^2}$, where β represents the coefficient associated with any form factor, it is that the exponential factor cuts the form factors above a certain value of Q^2 . Depending on the value of β , the parametrizations of the form factors can fall slower or faster, but decrease after a certain value of Q^2 . The polynomial factor can change the threshold of the falloff with Q^2 , but at some point the exponential factor dominates. A simple example of the exponential falloff effect is shown in Fig. 2, for the function R_{SM} when $Q^2 > 1.5 \text{ GeV}^2$. Since in that case, the value of β for G_C is larger than the value for G_E ($\beta = 3.33 \text{ GeV}^{-2}$ to be compared with $\beta = 1.31 \text{ GeV}^{-2}$), it is expected that R_{SM} falls to zero faster than R_{EM} , as we can see in the $Q^2 > 1.5 \text{ GeV}^2$ region. [We also need to take into account the falloff of G_M . The magnetic form factor G_M , is however regulated by a very small value, $\beta \simeq 0.2 \text{ GeV}^{-2}$, according with the MAID2007 parametrization].

Another disadvantage of the use the MAID-type parametrizations is the extension of the large Q^2 region, where the MAID parametrizations cannot be compared with the expected leading order power laws of pQCD (apart from logarithmic corrections) [45].

We then propose new parametrizations for the amplitudes and form factors, that differs from the MAID form, and corrects the high Q^2 behavior of the MAID parametrizations. As example, we will use the $\gamma^*N \rightarrow \Delta(1232)$ transition, since it is the transition with more

accurate data at large Q^2 , and can therefore be tested with more precision. The methods proposed can, however, be generalized for other transitions.

We divide our analysis into the magnetic form factor G_M (or amplitude M_{1+}) and into the quadrupole form factors G_E and G_C .

A. Magnetic form factor (G_M)

In the $\gamma^*N \rightarrow \Delta(1232)$ transition, we can represent the magnetic form factor G_M in terms of the magnetic amplitude M_{1+} , using $G_M = F_+ M_{1+}$, according with Eq. (3.10), where $M_{1+} = -(A_{1/2} + \sqrt{3}A_{3/2})$.

In the original MAID2007 parametrization, M_{1+} is represented by

$$M_{1+} = \frac{|\mathbf{q}|}{K} G_D \tilde{M}_0, \quad (5.1)$$

where $\tilde{M}_0 = a_0(1 + a_1 Q^2)e^{-a_4 Q^2}$. We now propose the form

$$\begin{aligned} M'_{1+} &= \frac{1}{\sqrt{1+\tau}} M_{1+} \\ &= \frac{M_R + M}{2M_R} \frac{\sqrt{Q_-^2}}{K} G_D \tilde{M}_0. \end{aligned} \quad (5.2)$$

The parametrization (5.2) has two main advantages compared to the original form. The first advantage is the inclusion of the factor $\sqrt{Q_-^2}$, which it will be canceled by the factor $F_+ \propto 1/\sqrt{Q_-^2}$, in the conversion from amplitudes to form factors. Since the factor $\sqrt{Q_-^2}$ is eliminated in the conversion to the form factors, we obtain simpler expressions for the form factors. The second advantage is the parametrization of the very large Q^2 region in a form more compatible with the power laws of pQCD [45], given by $M'_{1+} \propto 1/Q^3$, as we explain next.

From Eq. (5.2), we can immediately conclude that, $\sqrt{Q_-^2} G_D \propto 1/Q^3$, for large Q^2 . Thus, in order to obtain the expected $1/Q^3$ falloff for M'_{1+} , it is necessary that \tilde{M}_0 behaves as a constant, meaning that $\tilde{M}_0 = \mathcal{O}(1)$, for very large Q^2 . Since the function M_0 includes an exponential factor, it is obvious that we cannot have $\tilde{M}_0 = \mathcal{O}(1)$. We can correct this limitation replacing \tilde{M}_0 by an analytic expression that is close to the MAID form in the range of validity of the parametrization, $Q^2 = 0-10 \text{ GeV}^2$, but behaves like a constant for much higher Q^2 . This goal

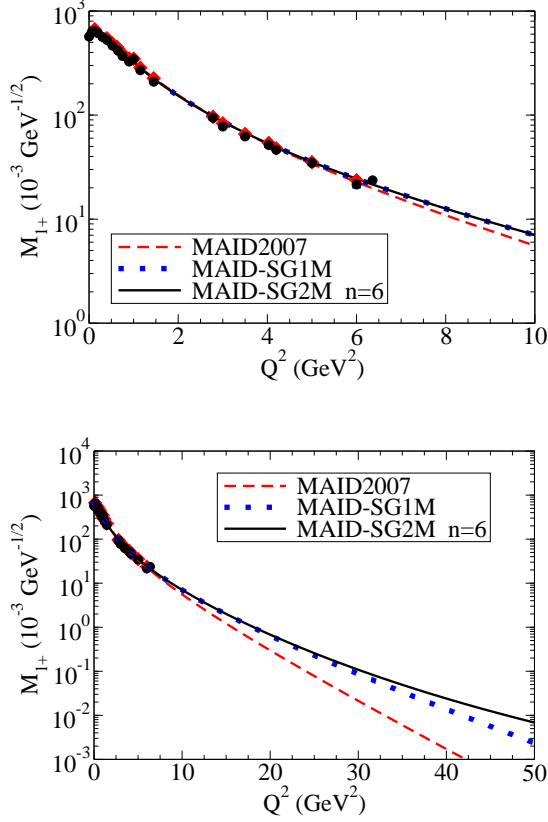


FIG. 10: $\gamma^* N \rightarrow \Delta(1232)$ transition. Magnetic amplitude M_{1+} compared with the MAID2007 parametrization and two alternative parametrizations (MAID-SG1M and MAID-SG2M). See discussion in the text. Data from MAID analysis (diamonds) [15, 16] and Ref. [22] (circles).

can be achieved with the replacement

$$\begin{aligned}
 \tilde{M}_0 &= a_0 \frac{1 + a_1 Q^2}{e^{a_4 Q^2}} \\
 &= a_0 \frac{1 + a_1 Q^2}{1 + a_4 Q^2 + \frac{1}{2!} a_4^2 Q^4 + \frac{1}{3!} a_4^3 Q^6 + \dots} \\
 &\rightarrow a_0 \frac{\sum_{k=0}^n \frac{(a_1 Q^2)^k}{k!}}{\sum_{k=0}^n \frac{(a_4 Q^2)^k}{k!}}, \quad (5.3)
 \end{aligned}$$

where $n \geq 1$ is an integer. In the last line, we *expanded* the factor $(1 + a_1 Q^2)$, using the exponential series, and truncated the exponential factor in the denominator, in the same order. Using the replacement (5.3), we obtain a simple rational function that converges to a constant for very large Q^2 . The dependence $M'_{1+} \propto 1/Q^3$ for very large Q^2 is then naturally generated.

Note that, the truncation of the exponential series in the denominator is particularly convenient, as far as it does not induce any singularity in the region $Q^2 < 0$. This can be assured if we restrict the expansion to even powers of n , as discussed in Appendix in detail.

The results of the MAID2007 parametrization for M_{1+}

are presented in Fig. 10. In addition to the MAID2007 parametrization defined by Eq. (5.1), where $a_4 = 0.23 \text{ GeV}^{-2}$, we consider a modification of the MAID2007 parametrization given by Eq. (5.2), with the replacement $a_4 \rightarrow 0.15 \text{ GeV}^{-2}$. We label this new parametrization as MAID-SG1M (M stands for magnetic amplitude). In the upper panel of Fig. 10, one can see, that, the new parametrization also gives a very good description of the data. We can then conclude that, Eqs. (5.1) and (5.2) provide equivalent parametrizations of the data, in the region $Q^2 = 0-10 \text{ GeV}^2$.

Finally, in order to check if a consistent description of the data is possible replacing the factor \tilde{M}_0 by a rational expression, as suggested by Eq. (5.3), we consider the modification of the MAID-SG1M parametrization by the expansion with $n = 6$. We label the new parametrization as MAID-SG2M. In the upper and lower panels of Fig. 10, one can see the comparison between MAID-SG1M and MAID-SG2M. In the upper panel, in the range $Q^2 < 10 \text{ GeV}^2$, the two models are almost not distinguishable. In the lower panel, when the scale of Q^2 is extended up to 50 GeV^2 , one can see that MAID-SG1M falls off faster than MAID-SG2M, as expected from the comparison between a rational and an exponential function. In the same graph, one can observe the linear behavior of the MAID2007 and MAID-SG1M parametrizations for $Q^2 > 20 \text{ GeV}^2$, due to the logarithmic scale used for M_{1+} . The graph also shows that, the difference between a parametrization based on powers of Q^2 (rational functions) and exponential functions, can in some cases, be disentangled only for very large Q^2 .

The parametrizations based on rational functions are efficient for moderate values of the argument $a_4 Q^2$, because the denominator in Eq. (5.3) converges smoothly, and faster than the expansion based on exponential series with negative arguments ($e^{-a_4 Q^2}$).

In the overall, we conclude, that the magnetic amplitude M_{1+} can be conveniently parametrized by the form (5.2), which behaves for large Q^2 as $M_{1+} \propto \tilde{M}_0/Q^3$. Combining this result with the rational parametrization given by Eq. (5.3), one obtains at the end a parametrization consistent with $M_{1+} \propto 1/Q^3$ and $G_M \propto 1/Q^4$.

The procedure used for the parametrization M_{1+} (M'_{1+}) can be used for the amplitudes E_{1+} (electric) and S_{1+} (scalar). The behavior of the amplitudes $A_{1/2}$, $A_{3/2}$ and $S_{1/2}$ for large Q^2 can also be estimated and/or extracted from the data. A note of caution about the results for very large Q^2 is in order. Since it is expected from pQCD arguments that $M_{1+} \simeq -E_{1+}$ for very large Q^2 [12, 45], a consistent parametrization of the data requires the correlation between the coefficients of both parametrizations. Since there are no experimental evidences of the scaling $M_{1+} \simeq -E_{1+}$, we cannot, at the moment, do more than estimate the expected shape of E_{1+} for very large Q^2 based on the knowledge of M_{1+} in the range $Q^2 \approx 10 \text{ GeV}^2$. Nevertheless, we can test if the quality of the fit for the form factors G_E and G_C , at low Q^2 , namely when $Q^2 < 1 \text{ GeV}^2$, can be extended for

MAID-SG0	r_0	r_1	r_2	r_3	r_4
G_E	21.64	-2.91	-5.72	-	1.79
G_C	23.75	-0.911	1.36	-	1.23
MAID-SG1	r_0	r_1	r_2	r_3	r_4
G_E	13.59	15.43	146.9	400.1	15.78
G_C	29.16	-1.20	3.30	0.690	2.47
MAID-SG2	r_0	r_1	r_2	r_3	r_4
G_E	13.84	2.220	7.44	14.79	6.13
G_C	22.33	4.66	-15.64	33.65	6.22

TABLE III: $\gamma^*N \rightarrow \Delta(1232)$ transition. Coefficients used in the calculation of G_E and G_C in the MAID-SG0 parametrization, defined by Eqs. (3.17)-(3.18); in the MAID-SG1 parametrization, defined by Eqs. (5.4)-(5.5); and MAID-SG2 parametrization, defined by Eqs. (5.6)-(5.7). The labels r_l ($l = 0, 1, 2, 3, 4$) holds for $r_l = b_l, c_l$. r_0 is in units $10^{-3} \text{ GeV}^{-1/2}$ ($C_0/K = 5.32 \text{ GeV}^{1/2}$). r_1 and r_4 are in units GeV^{-2} , r_2 in units GeV^{-4} , and r_3 in units GeV^{-6} . The values in bold are determined by Eqs. (3.14).

larger values of Q^2 .

B. Electric and Coulomb quadrupole form factors (G_E and G_C)

Inspired by Eq. (5.3), we check if similar extensions can be used for the form factors G_E and G_C , defined by Eqs. (3.17)-(3.18). For simplicity we restrict the discussion to the polynomial $(1 + r_1 Q^2 + r_2 Q^4 + r_3 Q^6)$ and the factors G_D , $e^{-r_4 Q^2}$, since the remaining factors are constant. As before $r_l = b_l, c_l$ ($l = 1, 2, 3, 4$).

The simplest extension, inspired by Eq. (5.3), is given by the replacement

$$(1 + b_1 Q^2 + b_2 Q^4 + b_3 Q^6) e^{-b_4 Q^2} G_D \rightarrow \frac{1 + b_1 Q^2 + b_2 Q^4 + b_3 Q^6}{1 + b_4 Q^2 + \frac{1}{2!} b_4^2 Q^4 + \frac{1}{3!} b_4^3 Q^6} G_D, \quad (5.4)$$

for G_E , and

$$(1 + c_1 Q^2 + c_2 Q^4 + c_3 Q^6) e^{-c_4 Q^2} G_D \rightarrow \frac{1 + c_1 Q^2 + c_2 Q^4 + c_3 Q^6}{1 + c_4 Q^2 + \frac{1}{2!} c_4^2 Q^4 + \frac{1}{3!} c_4^3 Q^6 + \frac{1}{4!} c_4^4 Q^8} G_D, \quad (5.5)$$

for G_C . Using Eqs. (5.4)-(5.5) we obtain the expected pQCD falloff: $G_E \propto 1/Q^4$ and $G_C \propto 1/Q^6$ for very large Q^2 [45]. We label this new parametrization for the quadrupole form factors as the MAID-SG1 parametrization.

Note that in the MAID-SG1 parametrization, we still include the dipole form factor G_D , where the cutoff $\Lambda^2 = 0.71 \text{ GeV}^2$, is extracted from the studies of the nucleon form factors. Since there is no particular reason

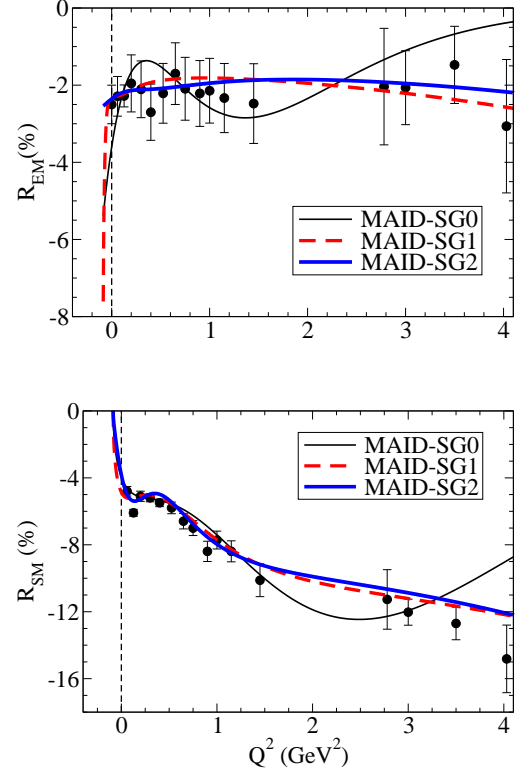


FIG. 11: $\gamma^*N \rightarrow \Delta(1232)$ transition. Ratios R_{EM} and R_{SM} given by the MAID-SG0, MAID-SG1 and MAID-SG2 parametrizations. Data from Ref. [22] (circles).

to expect that the scale of the form factors G_E and G_C is related to the scale of the nucleon form factors, we eliminate the factor G_D from the parametrizations for the quadrupole form factors, and transpose the $1/Q^4$ falloff to the remaining rational factors. A simple extension of the MAID-SG1 parametrization that excludes G_D is

$$(1 + b_1 Q^2 + b_2 Q^4 + b_3 Q^6) e^{-b_4 Q^2} G_D \rightarrow \frac{1 + b_1 Q^2 + b_2 Q^4 + b_3 Q^6}{1 + b_4 Q^2 + \frac{1}{2!} b_4^2 Q^4 + \frac{1}{3!} b_4^3 Q^6 + \frac{1}{4!} b_4^4 Q^8 + \frac{1}{5!} b_4^5 Q^{10}}, \quad (5.6)$$

for G_E , and

$$(1 + c_1 Q^2 + c_2 Q^4 + c_3 Q^6) e^{-c_4 Q^2} G_D \rightarrow \frac{1 + c_1 Q^2 + c_2 Q^4 + c_3 Q^6}{1 + c_4 Q^2 + \frac{c_4^2}{2!} Q^4 + \frac{c_4^3}{3!} Q^6 + \frac{c_4^4}{4!} Q^8 + \frac{c_4^5}{5!} Q^{10} + \frac{c_4^6}{6!} Q^{12}}, \quad (5.7)$$

for G_C . Equations (5.6)-(5.7) define the MAID-SG2 parametrization. As in the MAID-SG1 case, one obtains $G_E \propto 1/Q^4$ and $G_C \propto 1/Q^6$, for very large Q^2 .

In the parametrizations (5.4)-(5.5) and (5.6)-(5.7), it is important to ensure that no singularities are introduced in the denominator in the extension for the region

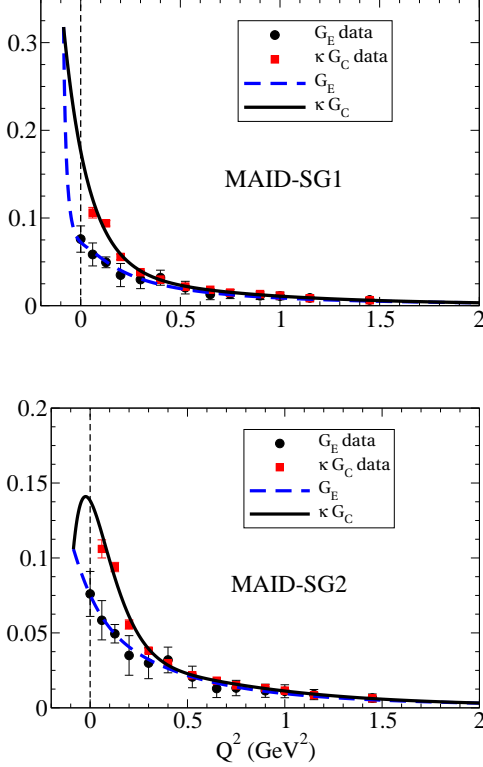


FIG. 12: Electric and Coulomb quadrupole form factors for the $\gamma^*N \rightarrow \Delta(1232)$ transition. G_C is multiplied by $\kappa = \frac{M_R - M}{2M_R}$. At the top: MAID-SG1 parametrization. At the bottom: MAID-SG2 parametrization. Data from Ref. [22].

$Q^2 < 0$. The analysis of the possible singularities is done in Appendix A. For the new parametrizations for G_C , it is possible to show that the functions are free from singularities, since the truncated expansion in powers Q^{2n} generates positive functions, (higher power Q^{2n} with even n), as shown in Appendix A 1. As for the parametrizations for G_E given by Eqs. (5.4) and (5.6), one needs to be more careful, since there is the possibility of singularities for larger values of b_4 , as discussed in Appendix A 2. We can however show that, the values of b_4 obtained in our fits, are consistent with parametrizations free of singularities (see the details of the discussion in Appendix A 2). In alternative to Eqs. (5.4) and (5.6), we can also define parametrizations of the functions G_E automatically singularity-free, if we remove or add a parameter to the expressions (5.4) and (5.6). This alternative is discussed in Appendix A 3.

As in Sec. III B, we tested if the MAID-SG1 and MAID-SG2 parametrizations, can give a good description of the data. Compared to Sec. III B, we increased the range of the data included in the fit from 2 GeV² to 4.1 GeV². As already discussed, there are discrepancies between the different analysis for large Q^2 . For this reason we avoid the use of $Q^2 > 4.1$ GeV² data.

In Sec. III B, we conclude, that, one should not expect

a good global description of the data simultaneously for small and large Q^2 , based on a MAID-type parametrization. To test the quality of the new parametrizations, MAID-SG1 and MAID-SG2, we extend first the previous MAID-SG parametrization to the range $Q^2 = 0$ –4.1 GeV². We label this new parametrization as MAID-SG0. The coefficients obtained in the refit are presented in the Table III, under the label MAID-SG0. It is interesting to note in the table that the best fit is obtained when $b_3, c_3 \simeq 0$.

The results for the ratios R_{EM} and R_{SM} for the three parametrizations are presented in Fig. 11. In the figure one can see that the description of the MAID-SG parametrization, that is good only up to 1.5 GeV², as shown in Fig. 2, it is improved up to about 3 GeV², with the MAID-SG0 parametrization. At the same time, one can confirm, from the graph for R_{EM} , that, a MAID-type parametrization (MAID-SG0), overestimates the value for $G_E(0)$ [underestimation of $R_{EM}(0)$].

We now look for the results obtained with the MAID-SG1 and MAID-SG2 parametrizations. The values of the coefficients determined by the best fit to the data, are also presented in the Table III. In Fig. 11, one can see, that, the MAID-SG1 and MAID-SG2 parametrizations give a very good description of the data, including the region $Q^2 > 2$ GeV². Qualitatively, the MAID-SG2 parametrization gives a better description of the G_E , G_C data (smaller chi-squared for G_E and G_C subsets, and smaller total chi-squared). The largest difference between the parametrizations MAID-SG1 and MAID-SG2 occurs for R_{EM} near the pseudo-threshold. The values of $R_{EM}(0)$, for both parametrizations, are very similar, but the results at the pseudo-threshold are very different. One has $R_{EM}(Q_{PS}^2) \simeq -5.34\%$ for MAID-SG0, $R_{EM}(Q_{PS}^2) \simeq -7.60\%$ for MAID-SG1 and $R_{EM}(Q_{PS}^2) \simeq -2.54\%$ for MAID-SG2.

The difference between the MAID-SG1 and MAID-SG2 parametrizations can be better observed in Fig. 12, where we present the results for G_E and G_C , where G_C is corrected by $\kappa = \frac{M_R - M}{2M_R}$. In this representation the difference between the two parametrizations becomes clear. the difference between the two parametrizations. [The graph for MAID-SG0 is similar to the graph for MAID-SG1]. One can now see that, the MAID-SG2 parametrization gives a smoother description of the data, with smaller values for G_E and G_C , near the pseudo-threshold. In contrast the MAID-SG1 parametrization shows a stronger variation of the form factors near the pseudo-threshold, that leads to a larger magnitude of $R_{EM}(Q_{PS}^2)$, and a larger difference to $R_{EM}(0)$.

Note, that, the MAID-SG2 parametrization has a behavior close to the MAID-SG parametrization (data up to 2 GeV²), as shown in Fig. 1, but contrary to MAID-SG, it provides an accurate description for larger Q^2 .

We can try to interpret the differences between the two global parametrizations: MAID-SG1 and MAID-SG2, recalling that MAID-SG2 gives the best fit. The large values obtained in the MAID-SG1 parametrization for G_E

and G_C , near the pseudo-threshold, are mainly a consequence of the factor G_D , included in the parametrizations (5.4)-(5.5). The function G_D is enhanced below $Q^2 = 0$ due to the pole $Q^2 = -0.71 \text{ GeV}^2$, inducing the large values for G_E and G_C near $Q^2 \simeq -0.09 \text{ GeV}^2$. We however note that, the factor G_D is not only responsible for large values of G_E and G_C , since the MAID-SG parametrization, restricted to the range $Q^2 = 0-2 \text{ GeV}^2$, leads also to smaller values for G_E and G_C , near the pseudo-threshold. When we increase the range of the fit, the factor G_D becomes more relevant. In any case, as discussed previously, since there is no reason to relate the function G_D to the $\gamma^* N \rightarrow \Delta(1232)$ quadrupole form factor data, a parametrization that avoids a reference to G_D and transfers the Q^2 dependence for the coefficients of the polynomial factors is preferable. For all the above reasons, MAID-SG2 is preferable over MAID-SG1.

C. Comparison with the literature

We now compare the parametrizations for G_E and G_C with alternative descriptions presented in the literature.

The ratio R_{SM} is calculated using pQCD in Ref. [46]. We do not compare our results directly with pQCD, since the result depends on a normalization at large Q^2 , and in the present work our main focus is the low and intermediate Q^2 region.

Alternative descriptions of G_E and G_C comes from the large N_c limit and from constituent quark models. Using the large N_c limit it is possible to relate the quadrupole form factors G_E and G_C with the neutron electric form factor G_{En} [47, 48], by

$$G_C(Q^2) = \sqrt{\frac{2M}{M_R}} M_R M \frac{G_{En}(Q^2)}{Q^2}, \quad (5.8)$$

$$G_E(Q^2) = \left(\frac{M}{M_R}\right)^{3/2} \frac{M_R^2 - M^2}{2\sqrt{2}} \frac{G_{En}(Q^2)}{Q^2}. \quad (5.9)$$

In the large N_c limit the form factors G_E and G_C appear as higher order corrections in $1/N_c$ to the leading order form factor G_M [47, 49]. The relations (5.8)-(5.9) are sometimes modified by the factor $(\frac{M_R}{M})^{3/2}$, which corresponds to $1/N_c^2$ correction [32, 50].

The derivation of Eqs. (5.8)-(5.9) is guided by the observation that within a $SU(6)$ spin-flavor symmetry model, the neutron would have a symmetric spatial distribution of charge, leading to $G_{En}(Q^2) = 0$. In addition, the electric and Coulomb quadrupole moments would both vanish [$G_E(0) = G_C(0) = 0$]. Non-zero results for G_{En} , $G_E(0)$ and $G_C(0)$ are then a consequence of the $SU(6)$ symmetry breaking [32, 51-53].

The relation (5.8) was derived for the first time in the context of a constituent quark model with two-body exchange currents [32, 52, 53]. Since the two-body currents are connected with diagrams involving $q\bar{q}$ pairs, those contributions can be regarded as the contributions of the

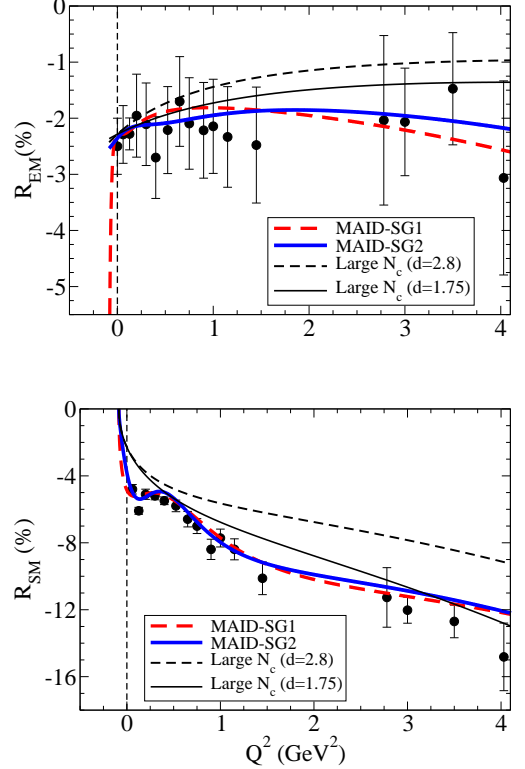


FIG. 13: $\gamma^* N \rightarrow \Delta(1232)$ transition. Ratios R_{EM} and R_{SM} given by two large N_c parametrizations characterized by the values of d . The MAID-SG1 and MAID-SG2 parametrizations are also presented for comparison. Data from Ref. [22] (circles).

cloud of quark-antiquark pairs. This mechanism is usually referred to as meson cloud effects. In the case of the nucleon and the first nucleon excitations, the dominant meson is the pion. Combining the low Q^2 expansion of the electric form factor, $G_{En}(Q^2) = -r_n^2 Q^2/6$, where r_n^2 is the neutron squared radius, one can show in the context of a constituent quark model with two-body exchange currents, that $G_E(0), G_C(0) \propto r_n^2$ [47, 51, 52]. It then becomes clear that, the mechanisms responsible for the symmetry breaking, which induce $r_n^2 \neq 0$, are also the mechanisms responsible for the non-zero quadrupole moments [32, 51-53]. The relation (5.8) is still valid when the three-body exchange currents are included for both observables, as can be shown using the expansion in $1/N_c$ [48, 54].

Although the relations (5.8)-(5.9) may be derived from a constituent quark model with two-body exchange currents, for simplicity we will refer those relations as large N_c (limit) parametrizations.

To represent the electric form factor of the neutron in Eqs. (5.8)-(5.9), one can consider the Galster parametrization [55]

$$G_{En}(Q^2) = -\mu_n \frac{a\tau_N}{1 + d\tau_N} G_D, \quad (5.10)$$

where $\mu_n = -1.913$ is the neutron magnetic moment,

$\tau_N = \frac{Q^2}{4M^2}$ and a, d are two parameters. The parameters a and d are related to the lowest radial moments of the neutron electric charge distribution. In particular a is determined by the second momentum r_n^2 (neutron squared radius) through $a = \frac{2M^2}{3\mu_n} r_n^2$. As for d , it is determined by r_n^2 and the fourth momentum r_n^4 [51, 52]. The MAID2007 parametrization for G_C is inspired by the Galster form (5.10) [15].

For the numerical evaluation of form factors G_E and G_C we consider two parametrizations with $a = 0.9$. One then has $r_n^2 \simeq -0.114 \text{ fm}^2$, close to experimental result $r_n^2 \simeq -0.116 \text{ fm}^2$ [26]. The best description of the neutron data is achieved with $d = 2.8$. A good description of the data can also be obtained with $d = 1.75$ [32].

The results from the (5.8)-(5.9) parametrizations combined with Eq. (5.10) for G_{En} are presented in Fig. 13. In the figure, one can notice that both parametrizations give a good description of the R_{EM} data, although the results of the parametrization with $d = 1.75$ are closer to the data. As for R_{SM} , the parametrization with $d = 1.75$ is also the one closer to the data, particularly for large Q^2 . For R_{SM} , however, both parametrizations, underestimate the low Q^2 data, in absolute value. We note that the ratio R_{SM} is usually estimated using parametrizations for G_M derived from $SU(6)$ or large N_c , as $G_M \rightarrow -\sqrt{2}G_{Mn}$, where G_{Mn} is the neutron magnetic form factor [32], or $G_M \rightarrow (F_{2p} - F_{2n})/\sqrt{2}$, where F_{2p}, F_{2n} are the Pauli form factor of the proton and neutron respectively [47]. In those estimates the magnitude of R_{SM} increases by about 15%, improving the agreement with the data. This observation also holds for R_{EM} ¹.

Going back to the discussion of R_{SM} , although there is some underestimation of the data at low Q^2 , and for the case $d = 2.8$ at large Q^2 , our results show that the parametrization (5.8) provides a good first estimate of the function G_C . Since Eq. (5.8) can be interpreted as the pion cloud contribution for G_C , we can conclude that the difference between the parametrization and the data can be the consequence of the valence quark contributions. In Ref. [31] it was shown, that a very good description of the G_E and G_C data can be obtained, when we add an extrapolation of the valence quark contributions from the lattice QCD data.

It is worth to mention that, the estimation of pion cloud contribution for G_C presented here is based on the Galster parametrization of the G_{En} data, which considers only two parameters. It is then possible that a more detailed fit to the G_{En} data, as the ones proposed in Refs. [57, 58], reveals also a more detailed structure of G_C for finite Q^2 .

Overall one can conclude that, the pion cloud contributions for the G_E and G_C form factors, given by

Eqs. (5.8)-(5.9), takes into account the dominate contribution of those form factors [32, 47]. Thus, contrary to the case of the magnetic dipole form factor G_M , the quadrupole form factors (electric and Coulomb) are not dominated by valence quark effects in the range $Q^2 = 1-4 \text{ GeV}^2$, but are instead dominated by pion cloud effects [32]. The magnitude of the valence quark contributions for the quadrupole form factors can be estimated as about 10-20% [20, 31, 53, 56]. Note that this magnitude is comparable with the difference between large N_c estimates and the data.

The results for R_{EM}, R_{SM} at low Q^2 can be better understood if we look for the limit $Q^2 = 0$. In that case we can conclude in the large N_c limit, that $R_{EM}(0) = R_{SM}(0) = \frac{1}{12\sqrt{2}} \left(\frac{M}{M_R}\right)^{3/2} \frac{M_R^2 - M^2}{G_M(0)} r_n^2$, is a consequence of $G_E(0) = \frac{M_R^2 - M^2}{4M_R^2} G_C(0)$ [47]. The correlation between the ratios however seems in conflict with the experimental data, since $R_{EM}(0) = -(2.5 \pm 0.5)\%$ and $R_{SM}(0.06 \text{ GeV}^2) = -(4.54 \pm 0.26)\%$. One can then conclude that, the large N_c limit underestimates G_C near $Q^2 = 0$. As mentioned, this can be a sign that the pure valence quark contributions may be more important for this form factor, as shown in particular in Ref. [31].

The analysis of the functions G_E and G_C at low Q^2 can be simplified if we look for the squared radius, that measures the slope of those functions at $Q^2 = 0$. The squared radius associated with the quadrupole form factors G_E and G_C is defined by

$$r_X^2 = -\frac{14}{G_X(0)} \left. \frac{dG_X}{dQ^2} \right|_{Q^2=0}, \quad (5.11)$$

where $X = E, C$. In the previous equation, the factor 14 replaces the factor 6 used in the leading order form factors (electric charge and magnetic dipole). This correction is the result of the expansion of the quadrupole operators in powers of Q^2 with the proper normalization [51, 59]. A direct consequence of Eq. (5.11) is that in the case of the large N_c parametrizations we can write the Coulomb quadrupole squared radius as $r_C^2 = \frac{7}{10} \frac{r_n^4}{r_n^2}$ [51].

Since the parametrizations MAID2007, MAID-SG1 and MAID-SG2 are analytic, both radius can be calculated using the coefficients of the parametrizations. The results are presented in Table IV. In the case of the large N_c parametrizations, the results for r_E^2 and r_C^2 are identical because both functions are correlated with G_{En} .

In Table IV we can note that the Coulomb squared radius, r_C^2 , is large in general, compared to the proton squared radius ($r_p^2 = 0.76 \text{ fm}^2$). The exception is the MAID-SG2 parametrization. The analysis of the values obtained for r_C^2 is interesting due to the suggestion that a large r_C^2/r_p^2 ratio is a manifestation of a large spatial extension of the charge distribution due to the $q\bar{q}$ pair distribution in the nucleon [51]. Recall that the $q\bar{q}$ cloud is the reason why G_{En}, G_E and G_C are non vanishing functions of Q^2 . Large values for r_C^2 reflect the increment of the size of the constituent quarks due to the $q\bar{q}$

¹ Assuming an error of 10% in a large N_c expansion of a form factor, for a term of the order $\mathcal{O}(1/N_c^2)$, one can expect an error of 20% in a ratio between two form factors.

	r_E^2 (fm ²)	r_C^2 (fm ²)
MAID2007	1.63	2.35
MAID-SG1	1.73	3.54
MAID-SG2	2.13	0.85
Large N_c ($d = 2.8$)	1.97	1.97
Large N_c ($d = 1.75$)	1.81	1.81

TABLE IV: $\gamma^*N \rightarrow \Delta(1232)$ transition. Results for the electric quadrupole and Coulomb quadrupole squared radius defined according to Eq. (5.11).

pair/meson cloud dressing [51, 52, 56]. In particular the results $r_C^2 \approx 2$ fm² can be interpreted as $r_C^2 \simeq r_\pi^2$, where $r_\pi = 1/m_\pi$ is the pion Compton wavelength, that characterizes the pion cloud distribution inside the nucleon [51].

The large values obtained for r_C^2 may then reflect the connection between the neutron charge distribution and r_C^2 . There is therefore a strong motivation to determine this radius experimentally [51, 52].

The previous discussion about r_C^2 can be generalized to r_E^2 (electric quadrupole squared radius), except that the range of the pion cloud effect is shorter in this case.

As mentioned, concerning the large extension of the pion cloud for G_C , the MAID-SG2 parametrization is the exception, since the value obtained for r_C^2 is closer to the proton squared radius ($r_p^2 = 0.76$ fm²). This result suggests that the extension of the pion cloud effect is shorter in this parametrization for G_C . As for G_E , we still expect a long distribution of the pion cloud.

To summarize the discussion about the quadrupole form factors G_E and G_C , we obtain the best description of the data, with a model compatible with the Siegert's theorem, when we use the MAID-SG2 parametrization. The MAID-SG2 parametrization gives a very good description of the form factors G_E and G_C at small Q^2 , with smoother functions near the pseudo-threshold, similarly to MAID-SG parametrization, but provides at the same time a very good description of the large Q^2 data.

The smoother behavior of the MAID-SG2 parametrization, is however characterized by a small value for r_C^2 , which suggests that the effect of the pion cloud is shorter for G_C . If the data is constrained by large values for r_C^2 , then MAID-SG2 does not provide the the best description of the data and the MAID-SG1 parametrization is preferable.

VI. SUMMARY AND CONCLUSIONS

In the present article we study the properties of the helicity amplitudes in the $\gamma^*N \rightarrow \Delta(1232)$ and $\gamma^*N \rightarrow N(1520)$ transitions, at the pseudo-threshold. One of the consequences of the pseudo-threshold limit is that the correlation between the electric amplitude E and the scalar amplitude $S_{1/2}$, in the long-wavelength limit

($|\mathbf{q}| \rightarrow 0$), which is usually refereed to as the Siegert's theorem.

We conclude, that, the analytic properties of the electromagnetic transition form factors imply that $\frac{E}{|\mathbf{q}|} = \sqrt{2}(M_R - M)\frac{S_{1/2}}{|\mathbf{q}|^2}$ for the $\gamma^*N \rightarrow \Delta(1232)$ transition and $E = 2\sqrt{2}(M_R - M)\frac{S_{1/2}}{|\mathbf{q}|}$ for the $\gamma^*N \rightarrow N(1520)$ transition. In the case of the $\gamma^*N \rightarrow \Delta(1232)$ transition, there is a additional $1/|\mathbf{q}|$ in both sides of the equation, relative to the form usually discussed in the literature, $E = \sqrt{2}(M_R - M)\frac{S_{1/2}}{|\mathbf{q}|}$. The result discussed in the present article is the consequence of the correlation between electric and Coulomb quadrupole form factors $G_E = \frac{M_R - M}{2M_R}G_C$. As for the $\gamma^*N \rightarrow N(1520)$ transition, one has in addition, the correlation between the transverse amplitudes $A_{1/2} = A_{3/2}/\sqrt{3}$, at the pseudo-threshold, which is equivalent to $G_M = 0$.

We tested the previous relations between amplitudes for the two transitions, and derived parametrizations of the available data, valid for small and large Q^2 , compatible with the constraints at the pseudo-threshold (Siegert's theorem).

The analytic form of our parametrizations can be used in future analysis of the $\gamma^*N \rightarrow N(1650)$ transition, similarly to the $\gamma^*N \rightarrow N(1520)$ transition [both are $\frac{1}{2}^+ \rightarrow \frac{3}{2}^-$ transitions].

Our parametrizations are compared directly with the MAID2007 parametrizations. The features of the MAID2007 parametrizations are discussed and the failure for the $\gamma^*N \rightarrow \Delta(1232)$ and $\gamma^*N \rightarrow N(1520)$ transitions, are explained in detail. In addition, we propose parametrizations similar to the usual MAID forms, that avoid the use of exponential factors. The new parametrizations are compatible with the low Q^2 data, the large Q^2 data, and also with the expected behavior of pQCD, for very large Q^2 . We conclude, that, the parametrizations based on rational functions of Q^2 are more appropriate for the description of the data in a wide region of Q^2 , as far as there are no singularities in the $Q^2 < 0$ region. This can be ensured, by making use of expansions of the exponential series with even powers of Q^2 in the denominator of the parametrizations for the helicity amplitudes or the transition form factors.

Our best parametrization for the $\gamma^*N \rightarrow \Delta(1232)$ amplitudes is consistent with smooth G_E and G_C form factors at low Q^2 , and near the pseudo-threshold, contrary to the MAID2007 parametrization. Our best parametrization provides a very good description of the low and large Q^2 data for the $\gamma^*N \rightarrow \Delta(1232)$ transition. The value obtained for Coulomb quadrupole square radius r_C^2 is close to the proton squared radius, suggesting that the effect of the pion cloud for G_C is shorter than in other parametrizations based on the $q\bar{q}$ effects.

As for the $\gamma^*N \rightarrow N(1520)$ transition, although there are some conflicts between different data analysis, it is possible to conclude that, different parametrizations of the different datasets, lead to the almost same extrapo-

lation for the low Q^2 region, and similar behavior near the pseudo-threshold.

The comparison between the parametrizations based on the Siegert's theorem, and estimates from valence quark models, suggests that, near the pseudo-threshold, processes beyond the impulse approximation are essential for the interpretation of the empirical data.

The methods proposed in the present article can be extended to the study of the helicity amplitudes and transition form factors associated with other nucleon excitations, as shown already, in particular for the $\gamma^*N \rightarrow N(1535)$ transition [13].

Acknowledgments

The author thanks Lothar Tiator for the useful discussions and Pulak Giri for useful suggestions. This work is supported by the Brazilian Ministry of Science, Technology and Innovation (MCTI-Brazil).

Appendix A: Study of the truncated exponential series

In this appendix, we discuss the possible singularities associated with the truncation of the exponential series used in the definition of the form factors G_E and G_C , for the MAID-SG1 and MAID-SG2 parametrizations, presented in Sec. VB.

We recall that those functions are based on the expansion

$$F(Q^2) = 1 + r_4 Q^2 + \frac{r_4^2}{2!} Q^4 + \dots + \frac{r_4^n}{n!} Q^{2n}, \quad (\text{A1})$$

where the value of n depends of the particular function/model under discussion.

We need to check if there are zeros in the function $F(Q^2)$. To simplify the analysis, we look for the worst case scenario, the point $Q^2 = Q_{PS}^2 = -(M_R - M)^2$. If there is no zeros, at the point $Q^2 = Q_{PS}^2$, there are no zeros for the values of Q^2 larger than Q_{PS}^2 . We then look for the polynomial function

$$P_n(x) = 1 - x + \frac{x^2}{2!} + \dots + (-1)^n \frac{x^n}{n!}, \quad (\text{A2})$$

where $x = r_4(M_R - M)^2$.

Since the function $P_n(x)$ is in the denominator of the functions G_E or G_C , it is important to know if there are singularities in those functions, given by the zeros of the function $P_n(x)$.

To study the possible zeros of $P_n(x)$, we divide the discussion into two cases: the case $n = 2, 4, 6, \dots$ (n even), and the case $n = 1, 3, 5, \dots$ (n odd).

n	x_0	$P_n(x_0)$
2	1	0.5
4	1.596	0.270
6	2.180	0.149

TABLE V: Point of minimum (x_0) and value for the function $P_n(x_0)$, for even values of n .

1. Even powers n

When $n = 2, 4, 6, \dots$, it is trivial to show that there are no solutions for $P_n(x) = 0$. We start by checking if there is a minimum for the function $P_n(x)$ when $x > 0$. The values of possible minima are determined by the zeros of the derivative $P'_n(x)$. The zeros of the derivative $P'_n(x)$, x_0 , are represented in Table V, together with the value of the function P_n at the same point. The derivative is calculated from $P'_n(x) = -P_{n-1}(x)$. From the table, we can conclude that the minimum of $P_n(x)$ is positive, therefore there are no singularities in the functions defined by $1/P_n(x)$, when n is even.

2. Odd powers n

We now consider the case $n = 3, 5, \dots$, when n is odd. It is easy to conclude that $P_n(x) = 0$, for some values of x , since we start with $P_n(0) = 1$, and the last coefficient of the sum (term in x^n) has a negative coefficient. Therefore for x large enough, $P_n(x) < 0$, and there is an intermediate point where $P_n(x)$ vanishes. There is therefore at least one singularity in the function $1/P_n(x)$. Since as discussed in the previous section we can write $P_n(x) = -P'_{n+1}(x)$, where $n - 1 = 2, 4, \dots$, is even, we know that the possible singularities are given by the points of zero of $P'_{n+1}(x)$, represented already in Table V.

Note, however, that below the zero of $P_n(x)$, we are free of singularities for $1/P_n(x)$. Therefore we can still use the function $P_n(x)$ with odd n , provided that $\frac{r_4}{(M_R - M)^2}$ is smaller than the value x_0 presented in Table V.

More specifically, in the case of the $\gamma^*N \rightarrow \Delta(1232)$ transition, there is no danger of using the function $P_3(x)$, provided that $r_4 < \frac{1.596}{(M_R - M)^2}$ or $r_4 < 18.6 \text{ GeV}^{-2}$. Similarly, we can use an expansion with $n = 5$, provided that $r_4 < \frac{2.18}{(M_R - M)^2} \simeq 25.4 \text{ GeV}^{-2}$. Other limits can be defined for higher powers n .

3. Alternative expressions for G_E

In the previous section, we concluded that, we can use the decomposition (A1) in the denominator of the functions G_E and G_C , under some conditions. The functions G_C for the MAID-SG1 and MAID-SG2 parametrizations,

given by Eqs. (5.5) and (5.7) can be used for any positive values of c_4 (that replaces r_4).

As for the parametrizations for G_E defined by Eqs. (5.4) and (5.6), the values of b_4 have to be constrained respectively to the limits $b_4 < 18.6 \text{ GeV}^{-2}$ and $b_4 < 25.4 \text{ GeV}^{-2}$, in order to avoid the singularities associated with the functions $P_3(x)$ and $P_5(x)$ respectively.

As discussed in the main text, the fits obtained in the present work are free from singularities, since b_4 is below the critical value. Nevertheless, in future, it may be more appropriate to define parametrizations for the function G_E , that are valid for all positive values of b_4 .

We therefore propose alternative expressions for G_E , that replace the form Eq. (5.4) for MAID-SG1 and Eq. (5.6) for MAID-SG2. For the parametrization MAID-SG1, we propose

$$G_E = \frac{C_0}{K} b_0 \frac{1 + b_1 Q^2 + b_2 Q^4 + b_3 Q^6 + b_5 Q^8}{1 + b_4 Q^2 + \frac{b_2^2}{2!} Q^4 + \frac{b_3^3}{3!} Q^6 + \frac{b_4^4}{4!} Q^8} G_D, \quad (\text{A3})$$

As for the parametrization MAID-SG2, we propose

$$G_E = \frac{C_0}{K} b_0 \times \frac{1 + b_1 Q^2 + b_2 Q^4 + b_3 Q^6 + b_5 Q^8}{1 + b_4 Q^2 + \frac{b_2^2}{2!} Q^4 + \frac{b_3^3}{3!} Q^6 + \frac{b_4^4}{4!} Q^8 + \frac{b_5^5}{5!} Q^{10} + \frac{b_6^6}{6!} Q^{12}}. \quad (\text{A4})$$

Compared to the expressions of Eqs. (5.4) and (5.6), we included an extra coefficient b_5 , adding some complexity to the parametrization. Alternatively, we can drop the last two terms in the numerator (terms with b_3 and b_5) and the last two terms in the denominator, generating simpler parametrizations of the function G_E , based on only 3 parameters (b_1, b_2 and b_4). The last choice can also be a good option, since the chi-squared associated with the G_E data is smaller (more accurate description) than the chi-squared associated with the G_C data. In this case the quality of the global fit is not compromised. As in the MAID-SG1 and MAID-SG2 cases, the new parametrizations are consistent with the falloff $G_E \propto 1/Q^4$, for large Q^2 .

-
- [1] I. G. Aznauryan *et al.*, Int. J. Mod. Phys. E **22**, 1330015 (2013) [arXiv:1212.4891 [nucl-th]].
 - [2] I. G. Aznauryan and V. D. Burkert, Prog. Part. Nucl. Phys. **67**, 1 (2012) [arXiv:1109.1720 [hep-ph]].
 - [3] G. Ramalho, M. T. Peña, J. Weil, H. van Hees and U. Mosel, Phys. Rev. D **93**, 033004 (2016) [arXiv:1512.03764 [hep-ph]]; G. Ramalho and M. T. Peña, Phys. Rev. D **85**, 113014 (2012) [arXiv:1205.2575 [hep-ph]].
 - [4] W. J. Briscoe, M. Dring, H. Habermann, D. M. Manley, M. Naruki, I. I. Strakovsky and E. S. Swanson, Eur. Phys. J. A **51**, 129 (2015) [arXiv:1503.07763 [hep-ph]].
 - [5] A. J. Buchmann, E. Hernandez, U. Meyer and A. Faessler, Phys. Rev. C **58**, 2478 (1998).
 - [6] C. Ciofi Degli Atti, Prog. Part. Nucl. Phys. **3**, 163 (1978).
 - [7] E. Amaldi, S. Fubini, and G. Furlan, *Pion-Electroproduction Electroproduction at Low Energy and Hadron Form Factor*, Springer Berlin Heidelberg (1979).
 - [8] D. Drechsel and L. Tiator, J. Phys. G **18**, 449 (1992).
 - [9] L. Tiator, Proceedings of the Workshop "Nucleon Resonances: From Photoproduction to High Photon Virtualities". October 2015, Trento, Italy.
 - [10] J. D. Bjorken and J. D. Walecka, Annals Phys. **38**, 35 (1966).
 - [11] R. C. E. Devenish, T. S. Eisenschitz and J. G. Korner, Phys. Rev. D **14**, 3063 (1976).
 - [12] H. F. Jones and M. D. Scadron, Annals Phys. **81**, 1 (1973).
 - [13] G. Ramalho, arXiv:1602.03444 [hep-ph]. To appear in Phys. Lett. B.
 - [14] L. Tiator and S. Kamalov, AIP Conf. Proc. **904**, 191 (2007) [nucl-th/0610113].
 - [15] D. Drechsel, S. S. Kamalov and L. Tiator, Eur. Phys. J. A **34**, 69 (2007) [arXiv:0710.0306 [nucl-th]].
 - [16] L. Tiator, D. Drechsel, S. S. Kamalov and M. Vanderhaeghen, Eur. Phys. J. ST **198**, 141 (2011) [arXiv:1109.6745 [nucl-th]]; L. Tiator, D. Drechsel, S. S. Kamalov and M. Vanderhaeghen, Chin. Phys. C **33**, 1069 (2009) [arXiv:0909.2335 [nucl-th]].
 - [17] G. Ramalho and M. T. Peña, Phys. Rev. D **89**, 094016 (2014) [arXiv:1309.0730 [hep-ph]].
 - [18] D. Drechsel and M. M. Giannini, Phys. Lett. B **143**, 329 (1984).
 - [19] G. Ramalho, M. T. Peña and F. Gross, Eur. Phys. J. A **36**, 329 (2008) [arXiv:0803.3034 [hep-ph]].
 - [20] G. Ramalho, M. T. Peña and F. Gross, Phys. Rev. D **78**, 114017 (2008) [arXiv:0810.4126 [hep-ph]].
 - [21] G. Ramalho and K. Tsushima, Phys. Rev. D **82**, 073007 (2010) [arXiv:1008.3822 [hep-ph]].
 - [22] V. Mokeev, https://userweb.jlab.org/~mokeev/resonance_electrocouplings/
 - [23] S. Stave *et al.* [A1 Collaboration], Phys. Rev. C **78**, 025209 (2008) [arXiv:0803.2476 [hep-ex]].
 - [24] N. F. Sparveris *et al.* [OOPS Collaboration], Phys. Rev. Lett. **94**, 022003 (2005) [nucl-ex/0408003]; J. J. Kelly *et al.*

- al.*, Phys. Rev. C **75**, 025201 (2007) [nucl-ex/0509004].
- [25] I. G. Aznauryan *et al.* [CLAS Collaboration], Phys. Rev. C **80**, 055203 (2009) [arXiv:0909.2349 [nucl-ex]].
- [26] K. A. Olive *et al.* [Particle Data Group Collaboration], Chin. Phys. C **38**, 090001 (2014).
- [27] G. Blanpied *et al.*, Phys. Rev. C **64**, 025203 (2001).
- [28] M. Weyrauch and H. J. Weber, Phys. Lett. B **171**, 13 (1986) [Phys. Lett. B **181**, 415 (1986)].
- [29] M. Bourdeau and N. C. Mukhopadhyay, Phys. Rev. Lett. **58**, 976 (1987).
- [30] S. Capstick and G. Karl, Phys. Rev. D **41**, 2767 (1990).
- [31] G. Ramalho and M. T. Peña, Phys. Rev. D **80**, 013008 (2009) [arXiv:0901.4310 [hep-ph]].
- [32] A. J. Buchmann, Phys. Rev. Lett. **93**, 212301 (2004) [hep-ph/0412421].
- [33] In Ref. [11], the Coulomb form factor G_C is defined with the difference of a sign, compared to our convention [2, 17].
- [34] We conclude, that, in this case, the difference between two functions $\mathcal{O}(1)$ leads to a function $\mathcal{O}(|\mathbf{q}|^2)$, as consequence of the relation between the amplitudes $A_{3/2}$ and $A_{1/2}$. A similar result was also observed in the study of the $\gamma^* N \rightarrow N(1535)$ helicity amplitudes [13]. See Ref. [13] for a more detailed explanation about the vanishing of the term $\mathcal{O}(|\mathbf{q}|)$.
- [35] V. I. Mokeev *et al.* [CLAS Collaboration], Phys. Rev. C **86**, 035203 (2012) [arXiv:1205.3948 [nucl-ex]].
- [36] V. I. Mokeev *et al.*, arXiv:1509.05460 [nucl-ex].
- [37] A. V. Anisovich, R. Beck, E. Klempt, V. A. Nikonov, A. V. Sarantsev and U. Thoma, Eur. Phys. J. A **48**, 15 (2012) [arXiv:1112.4937 [hep-ph]].
- [38] R. L. Workman, R. A. Arndt, W. J. Briscoe, M. W. Paris and I. I. Strakovsky, Phys. Rev. C **86**, 035202 (2012) [arXiv:1204.2277 [hep-ph]].
- [39] B. Julia-Diaz, T.-S. H. Lee, A. Matsuyama, T. Sato and L. C. Smith, Phys. Rev. C **77**, 045205 (2008) [arXiv:0712.2283 [nucl-th]].
- [40] E. Santopinto and M. M. Giannini, Phys. Rev. C **86**, 065202 (2012) [arXiv:1506.01207 [nucl-th]].
- [41] M. Ronniger and B. C. Metsch, Eur. Phys. J. A **49**, 8 (2013) [arXiv:1207.2640 [hep-ph]].
- [42] B. Golli and S. Širca, Eur. Phys. J. A **49**, 111 (2013) [arXiv:1306.3330 [nucl-th]].
- [43] V. I. Mokeev *et al.*, Phys. Rev. C **93**, 025206 (2016) [arXiv:1509.05460 [nucl-ex]].
- [44] U. Meyer, E. Hernandez and A. J. Buchmann, Phys. Rev. C **64**, 035203 (2001).
- [45] C. E. Carlson and N. C. Mukhopadhyay, Phys. Rev. Lett. **81**, 2646 (1998) [hep-ph/9804356]; C. E. Carlson and J. L. Poor, Phys. Rev. D **38**, 2758 (1988); C. E. Carlson, Phys. Rev. D **34**, 2704 (1986).
- [46] A. Idilbi, X. Ji and J. P. Ma, Phys. Rev. D **69**, 014006 (2004) [hep-ph/0308018].
- [47] V. Pascalutsa and M. Vanderhaeghen, Phys. Rev. D **76**, 111501 (2007) [arXiv:0711.0147 [hep-ph]].
- [48] A. J. Buchmann, J. A. Hester and R. F. Lebed, Phys. Rev. D **66**, 056002 (2002) [hep-ph/0205108].
- [49] E. E. Jenkins, X. Ji and A. V. Manohar, Phys. Rev. Lett. **89**, 242001 (2002) [hep-ph/0207092].
- [50] V. Pascalutsa, M. Vanderhaeghen and S. N. Yang, Phys. Rept. **437**, 125 (2007) [hep-ph/0609004].
- [51] A. J. Buchmann, Can. J. Phys. **87**, 773 (2009) [arXiv:0910.4747 [physics.atom-ph]].
- [52] P. Grabmayr and A. J. Buchmann, Phys. Rev. Lett. **86**, 2237 (2001) [hep-ph/0104203].
- [53] A. J. Buchmann, E. Hernandez and A. Faessler, Phys. Rev. C **55**, 448 (1997) [nucl-th/9610040].
- [54] A. J. Buchmann and E. M. Henley, Phys. Rev. D **65**, 073017 (2002).
- [55] S. Galster, H. Klein, J. Moritz, K. H. Schmidt, D. Wegener and J. Bleckwenn, Nucl. Phys. B **32**, 221 (1971).
- [56] A. J. Buchmann and E. M. Henley, Phys. Rev. C **63**, 015202 (2000) [hep-ph/0101027].
- [57] J. Friedrich and T. Walcher, Eur. Phys. J. A **17**, 607 (2003) [hep-ph/0303054].
- [58] J. J. Kelly, Phys. Rev. C **70**, 068202 (2004).
- [59] T. De Forest, Jr. and J. D. Walecka, Adv. Phys. **15**, 1 (1966).